UNIVERSITY OF CAMBRIDGE
Department of Engineering

Optimisation and design of a compressor for atmospheric resource extraction on Mars

Author Name: Sam Ross
Supervisor: Professor Nick Atkins
Date: 2023-06-01

I hereby declare that, except where specifically indicated, the work submitted herin is my own original work.

Signed _____Sam Ross_____ *date* __2023-06-01_____

Optimisation and design of a compressor for atmospheric resource extraction on Mars

Sam Ross, St Catharine's College

Humanity has long dreamt of exploring Mars, but any mission would be both complex and costly. One of the largest components of mission mass, and thus launch cost, is the propellant for the vehicle returning from Mars to Earth. For near-future vehicles like SpaceX's Starship, 1200 tonnes of propellant are required on Mars to return 200 tonnes of payload and vehicle to Earth. Transporting this much propellant from the surface of Earth would require over 180,000 tonnes of liquid methane and oxygen to be used. One approach for reducing this propellant requirement is to manufacture the return flight propellant on Mars from locally available resources. Since one tonne of equipment can produce many tonnes of propellant over its lifetime, the overall launch mass is reduced substantially. This approach is called In-Situ Resource Utilisation or ISRU.

Historic ISRU research efforts have focused on producing methane and oxygen from the Martian atmosphere (comprised of low-pressure carbon dioxide) and underground ice. However, this has largely been very small scale proof-of-concept hardware producing tens to hundreds of grams per hour. Refuelling a Starship-sized vehicle in a reasonable duration requires tens to hundreds of kilograms per hour, a three order-of-magnitude increase. This work carries out preliminary design of one subsystem of Martian ISRU, the atmospheric resource acquisition system, at a Starship-appropriate scale and investigates the potential for improvement over current technology using turbomachinery for compression and intercooling of the compressed gas.

To carry out the design of this complex ISRU subsystem, two design 'levels' were used. The high-level parameters such as mass flow and the number of intercooling heat exchangers were varied, and the required performance (pressure ratio, cooling power) of each component found. A component-level optimiser was then used to find the design for each compressor or heat exchanger that achieved the desired performance with the highest efficiency and lowest mass. The set of high-level parameters that maximised performance of the entire ISRU plant were found.

The overall system requirements were collated from climate data at proposed landing sites, the input states of existing systems and SpaceX daily mass flow requirements. In order to simplify the optimisation of components and selection of high-level parameters, the NASA-developed Equivalent System Mass (ESM) framework was used. This converts physical weight, power consumption, heat rejection and energy storage to a single value using equivalency factors based on the weight of appropriate auxiliary systems.

Many trade-offs exist in the choice of high-level parameters, which allow a designer to choose between different optimisation priorities. Varying the number of intercooling heat exchangers and compressors directly trades between physical weight and power/heat rejection. Increasing mass flow by running the atmospheric acquisition system for a limited portion of the day increases physical weight and power consumption, but reduces specific energy of compression through larger, higher-efficiency compressors. The choice of compressor type also allows for architecture-level performance tuning. This work considered axial, centrifugal and scroll compressors which operate across a range of available efficiencies, weights, volumetric flows and pressure ratios. The choice of compressor type at different points in the machine was subject to optimisation to allow this design space to be fully explored.

The component-level optimiser accepted the required performance of each component and optimised some descriptive variables to determine the set that minimised ESM. In practice, this optimiser worked to maximise efficiency, minimise weight and minimise intercooling heat exchanger pressure drop. For example, the axial compressor optimiser would accept a pressure ratio and inlet temperature and pressure from the high-level parameter calculation, and optimise across the work coefficient, flow coefficient and rotational speed. Each component had similar descriptive variables that were used by the component model to determine the ESM. For axial and centrifugal compressors these models used turbomachinery relationships to determine key geometric dimensions, a combination of empirical and explicit relationships for weight, and the Smyth and Miller topology selection plot to estimate efficiency. Scroll compressors used a volumetric flow scaling relationship for weight and a curve fit to literature data for efficiency. Intercooling heat exchangers used explicit relationships for weight, and channel flow correlations for gas side pressure drop and heat transfer coefficients. All component models were implemented in Python, with a Nelder-Mead (downhill simplex) optimiser used to find the ESM-minimising set of descriptive variables.

To validate the component models, a number of test cases from literature were analysed and the results compared. The axial compressor model performed with $< 10\%$ error for all key variables, as did the inlet geometry of the centrifugal compressor. Some elements of the centrifugal compressor outlet geometry showed more error, but all were fully explainable from the assumptions and simplifications made in the model. Centrifugal compressor efficiency was underpredicted, due to conservative assumptions about the achievable efficiency of the diffuser. However, a CFD validation of the centrifugal compressor model found approximate agreement. The intercooling heat exchanger model underpredicted heat transfer coefficients due to similar idealisations in the flow modelling. To further verify the models, it was confirmed that each descriptive variable was causing appropriate changes in component geometry, efficiency and weight.

The final optimised atmospheric resource acquisition system uses fifteen intercooling heat exchangers, six axial, eight centrifugal and seven scroll compressors. It operates at night only, condensing the atmosphere to store liquid carbon dioxide for use in a constantly running chemical process to produce methane and oxygen. This design has around four times less ESM than the current technology, with six times less specific compression energy. An investigation of the mass flow and intercooler number justified the choice of these high-level parameters as appropriately trading off physical mass, specific energy and heat exchanger pressure drop. A sensitivity analysis run on the component models showed expected impacts on the final ESM. Similarly, variations on the power and cooling equivalency factors used in ESM calculations shifted the optimiser's output to prioritise either power/cooling or mass appropriately.

Overall, this project has demonstrated the gains that may be achieved with the use of turbomachinery and intercooling for Martian atmospheric resource acquisition. By reducing the weight and energy requirements for producing carbon dioxide, future designs for ISRU plants can be made smaller and simpler and thus launch mass and cost reduced. Furthermore, any other ISRU processes that make use of carbon dioxide (including complex chemical synthesis and agriculture) can be considered higher merit due to the lower 'cost' of feedstock. This also demonstrates the effectiveness of designing space systems at full scale, where alternative technologies can be leveraged to reduce weight, efficiency and cost.

Contents

1 Introduction

1.1 Mars Exploration

Humanity has been exploring Mars with robotic spacecraft since the dawn of the space age, and has planned human missions for almost as long. Serious technical studies on the technology and architecture of crewed missions began in the 1960s [1], although NASA's 1993 Design Reference Mission [2] was the first coherent and well-funded proposal. This reference architecture provided the basis for subsequent development efforts and was later updated with Design Reference Mission 3.0 in 1997 and Design Reference Architecture 5.0 in 2009 [3]. These evolving documents represent the most developed and most studied plans for human Mars exploration.

Most Mars mission concepts assume a high launch cost - tens of thousands of dollars per kilogram delivered to Earth orbit, and several times this for launch to Mars. High launch costs lead to an extreme driver to reduce mission mass, to keep costs low. This justifies the use of highly mass-optimised systems and thus a high R&D cost.

However, this high launch cost paradigm is being rapidly altered by developments from new launch providers. Currently operating and near-future heavy lift rockets like the SpaceX Falcon Heavy and Blue Origin New Glenn are all capable of lifting 5-15 metric tonnes of payload to Mars with launch costs of 100-200 million dollars. This is almost an order of magnitude lower per-kilogram cost than the Space Shuttle-derived launch vehicles proposed in the Design Reference Missions.

Figure 1.1: A prototype of SpaceX's Starship/Super Heavy launch vehicle at the company's Texas manufacture and test facility [4].

This trend is accelerating rapidly with the maturation of SpaceX's Starship/Super Heavy launch vehicle, as shown in Figure 1.1. Starship is the first vehicle specifically designed for large-scale Mars landings to support exploration and settlement missions. Starship advertises a payload of 100-150 metric tonnes to Earth orbit and the capability for in-orbit refuelling [4]. This technique allows Starship's range to be extended with propellant launched on dedicated tanker vehicles. Since a Starship can be fully refuelled before departing to Mars it can transport up to 100 tonnes in a single trip. This is an order of magnitude increase over current vehicles, at a claimed price in the tens to hundreds of millions of dollars. Through this combination of large cargo capacity

and low costs, Starship has the potential to revolutionise large-scale exploration and settlement of space.

This new paradigm of large-scale low-cost exploration enables new approaches to the design of systems. Larger scales enable the use of different approaches for life support, propellant processing, power systems and so on, that would otherwise be uneconomical or excessively heavy at smaller scales. The low cost of launch also allows for heavier systems that instead reduce development cost by building on existing industrial experience, or by reducing the demands for high-cost components.

1.2 In-Situ Resource Utilisation

One essential component of any human Mars exploration mission is the return flight, allowing the crew to return to Earth. The return vehicle requires rocket propellant for the ascent from the Martian surface to orbit, and the subsequent flight from Mars to Earth. Due to the inherent efficiency limits of chemical rocket propulsion, around six kilograms of propellant are needed for each kilogram of payload returned from Mars to Earth [5]. Using Design Reference Mission-scale vehicles, this payload is around 50 tonnes [2] and so the required propellant mass is around 300 tonnes. For Starship, the total returned mass including vehicle structure is around 200 tonnes, and 1200 tonnes of propellant is needed.

Transporting this much propellant to Mars from Earth is impractical, both in terms of mission operations and launch costs. Just as propellant is needed to transport payload from Mars to Earth, additional propellant is also needed to travel from Earth orbit to Mars, and from the surface of Earth to Earth orbit. For each kilogram of material transported from Earth to Mars, around 131 kg of propellant must be used [4]. The 1400 tonnes of propellant and vehicle needed at Mars for a Starship mission would thus require 183,000 tonnes of propellant to be expended. The cost of this propellant and associated launch operations, and the mission complexity of launching over 50 Starships for refuelling, makes this solution untenable.

The alternative solution, which has been advocated by the vast majority of mission concepts, is In-Situ Resource Utilisation or ISRU. This makes use of locally available resources on the surface of Mars to manufacture propellants that can be used for the Earth return flight. As long as the ISRU system produces a greater mass of propellant over a nominal lifespan than its own mass, a net improvement in mission effectiveness will be achieved. The greater the ratio between mass produced and system mass, the greater a saving in launched mass will be achieved. For ISRU systems at the Design Reference Mission scale, a ratio of 3-15 is possible [6] - thus reducing the required launched mass for the given missions by the same ratio.

ISRU systems can produce a wide variety of products, but the main focus is on propellant production since this is the heaviest single consumable on a typical mission. Propellant ISRU on Mars was pioneered as a concept by Ash et al in 1978 [7] and popularised by Zubrin's Mars Direct mission concept in 1996 [8] (which was greatly expanded upon by NASA into the Design Reference Mission). The majority of concepts use methane and oxygen as rocket propellants, since 95% of the propellant mass is available in the Martian atmosphere in the form of carbon dioxide. While Zubrin advocates for the importing of hydrogen to reduce complexity and power requirements, many modern proposals use water from ice deposits to produce this hydrogen in situ. This latter method is presumed for Starship, with the candidate landing sites chosen on the basis of presumed ice reserves [9].

A summary of the fundamental subsystems required for propellant ISRU are shown in Figure 1.2. Both carbon dioxide and water must be extracted from their local forms: the Martian atmosphere

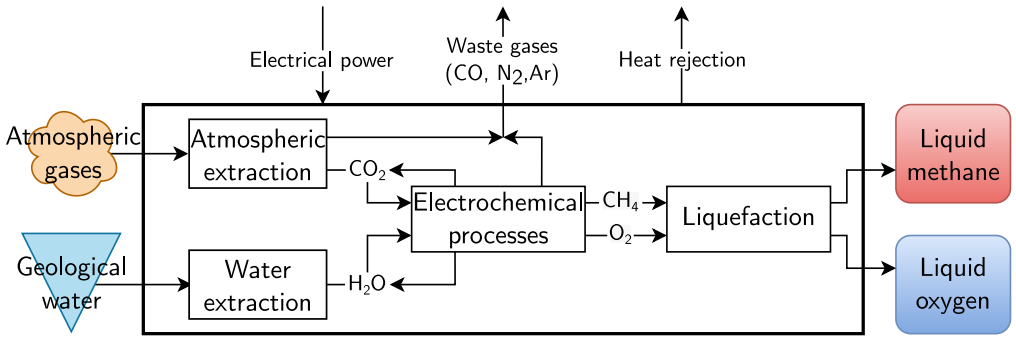

Figure 1.2: Subsystems within a generic methane-oxygen propellant production system for Mars

and geological reserves of ice or hydrated minerals respectively. All ISRU systems share a central chemical processing stack to convert these feedstocks to methane and oxygen - commonly using a Sabatier process reactor and electrolysis cell. Real chemical processes are not perfect and do not convert 100% of feedstock to product, represented by the water and carbon dioxide loop visible, and may also produce side products like carbon monoxide which can be rejected. Any propellants produced are in the gaseous phase and so must be liquefied to cryogenic temperatures before long-term storage. The process as a whole requires electrical energy, and rejects heat from exothermic chemical reactions and general inefficiencies.

In future, with Starship and similar very large vehicles becoming operational for Mars missions, the scale of ISRU systems must dramatically increase. Fuelling Starship for Earth return over a 500-day surface stay requires a propellant flow of almost three metric tonnes per day. This is more than 30 times the scale required for either the original Design Reference Mission or the updated Design Reference Architecture 5.0. This means that existing designs must be scaled up 30 times to meet the requirements of Starship

1.3 Atmospheric Resource Utilisation

All proposed Martian ISRU systems take advantage of atmospheric carbon dioxide as the source of both carbon and oxygen in methane-oxygen propellant. Since the atmospheric pressure on Mars is below 1 kPa, it is necessary to compress the intake gas by a factor of several hundred before it can be used in a practical electrolyser or chemical reactor. Achieving this compression with an efficient, lightweight system is the primary challenge of atmospheric resource acquisition subsystems for ISRU. Many designs also include provisions for the removal of contaminants like dust and trace gases. Three approaches have been considered historically, each outlined below

However, all currently explored systems operate at scales far below that required for Starship missions. Figure 1.3 shows a survey of 14 different atmospheric resource acquisition systems analysed or tested between 1978 and 2022. The highest mass flow considered was 619 g/h and the lowest specific energy was 3150 kJ/kg of carbon dioxide compressed. The change in enthalpy between Martian ambient conditions and a useful output state (500 kPa, 250 K) is 41 kJ/kg, meaning the best available system is operating with just 1.3% efficiency. This performance floor is marked in red in Figure 1.3. To refuel Starship over the desired 500 day period requires around 1000 kg of carbon dioxide per day or 40.6 kg/h, 65 times greater than the largest system. The target operating range for Starship is marked in Figure 1.3 in green - mass flow must exceed 40.6 kg/h, and specific compression energy must be as low as possible.

The early pioneers of Martian ISRU selected cryofreezers as the optimal approach for very small-scale carbon dioxide purification and pressurisation. This was first proposed by Ash [7], reiterated by Zubrin and later developed by teams at both NASA [10] and Lockheed Martin [14]. The

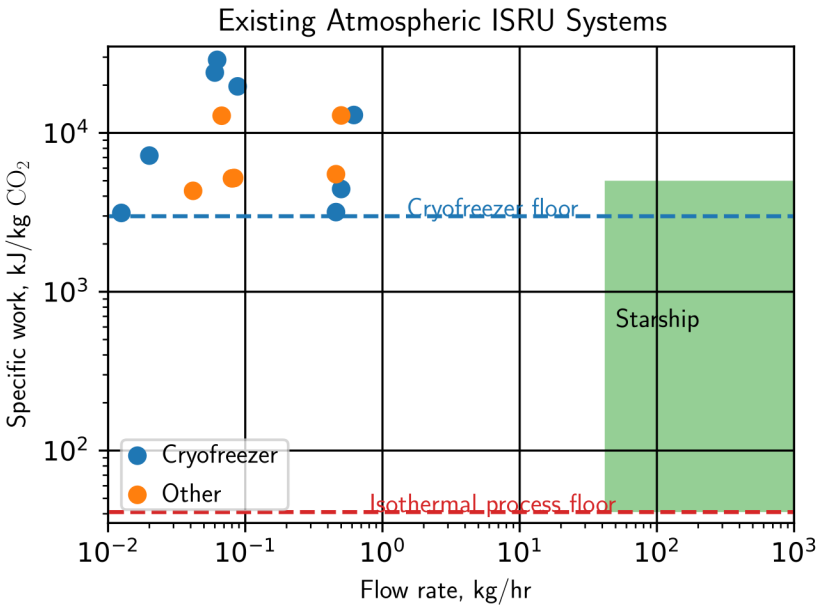

Figure 1.3: Performance of atmospheric resource acquisition systems available in the literature, compared to the performance floor of cryofreezers with realistic coefficients of performance (see below) and the true performance floor of isothermal compression. The target region for Starship is shown in green. Data points from [7, 10–19]

cryofreezer concept relies on the fact that carbon dioxide freezes at around 50 K below Martian ambient conditions, allowing collection of solid carbon dioxide inside a cooled chamber. The chamber can then be sealed, heated and the carbon dioxide sublimates or melts isochorically to produce a high pressure fluid. The chamber is cooled by a low-temperature helium cryocooler.

Cryofreezers all share mechanical simplicity (the only moving parts exposed to Martian atmosphere are a small number of valves) and can be scaled to almost arbitrarily small sizes, but all also suffer poor energy efficiency. Freezing carbon dioxide at Martian pressures releases a specific energy of around 600 kJ/kg. Cryocoolers working in the required temperature ranges suffer from extremely low coefficients of performance of 0.2 or lower, meaning the energy requirement for cryofreezers is at least 3000 kJ/kg. This performance floor is marked in Figure 1.3 in blue. The poor performance of cryocoolers and high enthalpy of fusion of carbon dioxide fundamentally limits the efficiency achievable by cryocoolers to just a few percent relative to the thermodynamic minimum.

Some sources, including Design Reference Architecture 5.0, have proposed adsorption pumps as an alternative to cryofreezers. These use a solid or liquid adsorbent material which is loaded with carbon dioxide from the atmosphere, and are then heated to reject the carbon dioxide into a small volume thus achieving simultaneous pressurisation and purification. Adsorption pumps are as mechanically simple as cryofreezers, needing only heaters and valves to operate, and remove the need for inefficient cryocoolers. However, the relatively slow reaction, high thermal capacity of adsorbent and low capacity for carbon dioxide drives adsorption beds to be heavy and high-energy. Rapp [20] reports a microchannel adsorption pump design with a specific work of 5300 kJ/kg of carbon dioxide, a lower efficiency than tested cryofreezer designs, and an absorbent mass of 640 grams per kilogram of carbon dioxide per day.

In recent years, a third alternative for atmospheric compression has become increasingly popular - mechanical compression using either dynamic or positive displacement compressors. While

initially rejected by Ash due to perceived high weight and low efficiency at small scales, positive displacement pumps are the focus of increasing interest and research for small- to medium-scale systems. This has culminated in the successful field testing of the MOXIE experiment on the Perseverance Mars rover. This uses a scroll compressor designed by Air Squared to deliver 83 grams of carbon dioxide per hour at a pressure of 1 bar to a high-temperature solid-oxide electrolysis cell to produce oxygen and carbon monoxide. As of August 2022, MOXIE has produced 194 grams of oxygen over 9 hours of operation [12] - a hugely impressive technical achievement, but far short of the requirements for providing propellant for a human Mars mission.

The work of MOXIE has been extended by Hinterman [21], who detailed the design of a MOXIE-derived oxygen plant using solid oxide electrolysis. This work proposed the use of a single large scroll compressor with a lower pressure ratio than MOXIE to provide feedstock for an electrolyser. Hinterman's work represents the highest mass flow design study for an atmospheric ISRU system available in the literature, with a mass flow of 15 kg/h of carbon dioxide. This also has the lowest specific energy by far of any concept proposed, just 400 kJ/kg carbon dioxide, but delivers a much lower pressure (18 kPa) than the bulk of methane-oxygen propellant production designs (typically 100 kPa or higher).

1.4 Summary and Research Questions

In order to carry out missions at the Starship scale, the entire ISRU process - including atmospheric resource acquisition - must be carried out at large scale and high efficiency. From the information of Figure 1.3, it is clear than current technology for atmospheric ISRU is unsuitable for Starship-scale missions. Existing adsorption pumps, cryofreezers and small mechanical pumps have flow rates at least an order of magnitude too low for practical use in a large-scale mission, with extremely poor efficiencies.

The research questions are thus:

- What technology and architecture is most suitable for the atmospheric resource acquisition system of a Starship-scale mission?
- What is the likely efficiency of such a system, and how sensitive is the architecture to the design assumptions?

This work addresses this question by carrying out preliminary design of a a Martian atmospheric resource acquisition system at the scale required for Starship. It applies two approaches that are novel to the application, multistage turbomachinery and intercooling, to achieve a four-fold increase in performance at the appropriate mass flows for a successful Starship mission to Mars. If realised, this technology could provide a fundamental building block of the system that carries humans to the red planet and brings them safely home.

2 Modelling Context

The role of any designer is to maximise value: i.e. meet or exceed the functionality of the system requirements while minimising costs. For such a highly multivariate ISRU system, this is not a simple task. First the requirements and operating context must be established for the atmospheric resource acquisition system. This allows a sensible definition of cost to be made. Once this context is laid out, the design and optimisation of the system can begin.

2.1 System Requirements

The goal for the atmospheric resource acquisition system is to provide the feedstock to the downstream electrochemical processing stack, allowing for conversion of carbon dioxide to methane and oxygen with the addition of water. The input requirements of this downstream stack sets the requirement for the outputs of the atmosphere acquisition system. The quantitative requirements are given in Table 2.1. Inlet conditions are also stated, and are justified further in Section 2.3.

The mass flow required of the atmospheric acquisition system is 1000 kg of carbon dioxide per day. This reflects the requirement to entirely refuel the Starship vehicle within 500 days on the Martian surface. However, the mass flow per second is a free variable - reflecting the fact that the atmospheric system may operate for only parts of the day, rather than continuously.

The output pressure is similarly a soft requirement, with an advised minimum value based on designs in the literature. A higher pressure is desirable in the chemical reactor to drive the methane-producing reaction to higher yields, although this is balanced by the increasing pumping power and pressure vessel weight. A reactor pressure of 500 kPa has been experimentally found to be effective for methane production [19] so this is considered the minimum output pressure for the atmospheric resource acquisition system.

Variable	Value	Source
Propellant mass flow	1800 kg/day	Required to refuel Starship in 500 days [22]
CO_2 flow	1000 kg/day	Ratio for methane-oxygen production [22]
CO_2 output pressure	>500 kPa	Based on existing systems[19]
Atmosphere inlet pressure	750-820 Pa	Mars Climate Database, daily range[23]
Atmosphere inlet temperature	180-225 K	Mars Climate Database, daily range[23]

Table 2.1: Requirements for a Starship-scale ISRU system, and particularly the atmospheric resource acquisition system

2.2 System Merit Evaluation

While conceptually simple, describing the performance of an ISRU system is not simple because of the number of forms of energy and mass crossing the system boundary, and thus the number of ways to evaluate the performance. The ISRU process of interest to this work deals with many mass flows of input, intermediate, waste, byproduct and product materials as well as electrical and thermal energy flows. The system carrying out the process also possesses a weight and occupies a volume on the spacecraft. To best approach the design task, a single performance evaluation merit is sought.

In order to evaluate the relative merit of systems while considering each of these flows crossing the system boundary, the framework of Equivalent System Mass (ESM) can be used. Originally developed by NASA to compare life support system architectures [24], it is also ideally suited for evaluating ISRU systems and subsystems. ESM takes four key properties of the system in

a representative operating mode: mass, power consumption, cooling power and stored energy requirement. Each of the non-mass properties are multiplied by a scaling factor to find their mass equivalents. The equivalent masses are then summed to find the approximate mass including all auxiliary systems of power generation and heat rejection.

The value of these scaling factors have been determined by the ESM authors from the properties of various auxiliary systems - either determined from a detailed analysis or using reference values. For instance, the scaling factor for power is determined from the mass of the power generation system per unit of output. The choice of ESM scaling factors thus requires implicit choices about the power generation, thermal management and energy storage systems of the mission. The NASA Life Support Basic Values and Assumptions Document (BVAD) [5] includes reference values for several alternatives of each of the auxiliary systems (power generation, cooling and energy storage). No scaling is required for mass. Where not otherwise specified, the scaling factors below are sourced from BVAD.

The methods generally considered viable for power generation on the surface of Mars are solar, nuclear decay heat and nuclear fission. Nuclear decay heat is proven to work on the Martian surface but is comparatively inefficient and heavy. Nuclear fission has relatively high power density and works at large scales, but is extremely complex and risky for an early Mars mission. Thus, only solar power is considered in this analysis. Solar power has a scaling factor varying from 149 kg/kW_e to 10 kg/kW_e [5], (depending on the solar cell and structural weight of the relevant architecture) and requires energy storage to function overnight.

The traditional method for rejecting heat in space is thermal radiators. These maintain a temperature above the environment, thus rejecting energy through infrared radiation. The scaling factor for radiators on the Martian surface in the BVAD document is 145-121 kg/kW_{th} with a coolant temperature of 278 K [25]. Other methods of heat rejection may exist, such as vapour compression heat pumps or open-loop coolers using atmospheric gas, but these are significantly more complex and so are not considered.

Many approaches exist for energy storage, but only fuel cells and batteries have extensive heritage in spaceflight applications. The best lithium-polymer or lithium-ion batteries listed in the BVAD document can achieve an energy density of 200 Wh/kg, and thus a scaling factor of 5 kg/kWh. Regenerative fuel cells may achieve slightly better performance, around 4-4.5 kg/kWh, but also add substantial complexity. Values for batteries are thus used for the remainder of this work.

Property	Lower value	Upper value
Mass		**1** kg/kg
Power	50 kg/kW_e	**149** kg/kW_e
Cooling	75 kg/kW_{th}	**121** kg/kW_{th}
Energy storage	5 kg/kWh	**5** kg/kWh

Table 2.2: Upper and lower values for ESM scaling values used in this work, with default values values in bold. All values from the BVAD document [5]

While the values of ESM scaling factors imply design choices about the auxiliary systems supporting the atmospheric resource acquisition system, it should be noted that the numerical values chosen are not fixed properties. The exact "mass costs" of the power, cooling and energy storage cannot be determined until the complete spacecraft is designed. Indeed, these mass costs are unlikely to be linear for certain subsystems like power conditioning equipment and coolant circulating pumps. This work uses a simple framework to assess the the sensitivity of the design

to the ESM scaling factors. The entire design framework accepts an arbitrary vector of ESM factors, which was varied between the high and low values of Table 2.2 and the differing outputs of the optimiser assessed.

As well as providing a route to evaluate the relative merits of different systems, the ESM approach allows the expression of the relative importance of different properties of the system. With the default scaling factors of Table 2.2, power generation has a higher scaling factor than cooling. Reducing power consumption by a given percentage would therefore have a greater effect on ESM than reducing cooling by the same percentage. In this way, the ESM scaling factors directly report that power reduction should be a higher priority than cooling reduction, all else being equal.

By extension, this method also serves as a very effective way to directly adjust the 'weighting' given to different performance characteristics in a design system. For instance, a low scaling factor for power but a high one for cooling would heavily penalise designs that require extensive cooling, but be more accepting of poor efficiency and high power consumption. In this way, ESM provides a very simple way to vary design and optimisation prioritisation for different aspects of the system performance.

For this reason, as well as simplicity of calculation, Equivalent System Mass was used as the means of calculating the system performance both within the design system developed in this work.

2.3 Martian Atmospheric Properties

The atmospheric resource acquisition system must be designed to operate effectively on the surface of Mars. The Martian atmosphere is composed of 95% carbon dioxide by molar ratio, with argon and nitrogen composing an additional 4.3% [21]. The remaining trace gases include oxygen, carbon monoxide and water. The ambient temperature varies diurnally and seasonally, but generally falls into a range from 170 K to 260 K [23]. The atmospheric pressure is low compared to Earth, below 1 kPa across a majority of the planet's surface.

As on Earth the conditions of the Martian atmosphere vary with location, weather, time and date. The conditions used in this study are from the sites officially proposed for Starship landings [9], with atmospheric properties found from the Mars Climate Database [23]. Atmospheric properties spanning a representative Martian year were found at 1-hour intervals at three locations representing the groups of proposed landing sites - Erebus Montes, Arcadia Planitia and Phlegra Montes. The parameters for each site are given in Table 2.3, and the envelope of conditions expected is shown in Figure 2.1. The variation over a single local day is shown, with a maximum and minimum envelope of conditions expected throughout a complete Martian year. This data does not account for extraordinary weather conditions including dust storms.

Site	Latitude	Longitude	Altitude	Temperature	Pressure
Erebus Montes	39 °N	193 °E	-3900 m	200.3 K	820.6 Pa
Arcadia Planitia	39 °N	202 °E	-3900 m	198.6 K	820.0 Pa
Phlegra Montes	36 °N	162 °E	-2300 m	199.0 K	702.0 Pa

Table 2.3: The three proposed landing areas, with their associated annual average properties

When designing the atmospheric resource acquisition system, an appropriate daily average of properties should be used. For a given target output pressure, the design input pressure should be the lowest reasonably encountered - thus ensuring the design output is always achieved.

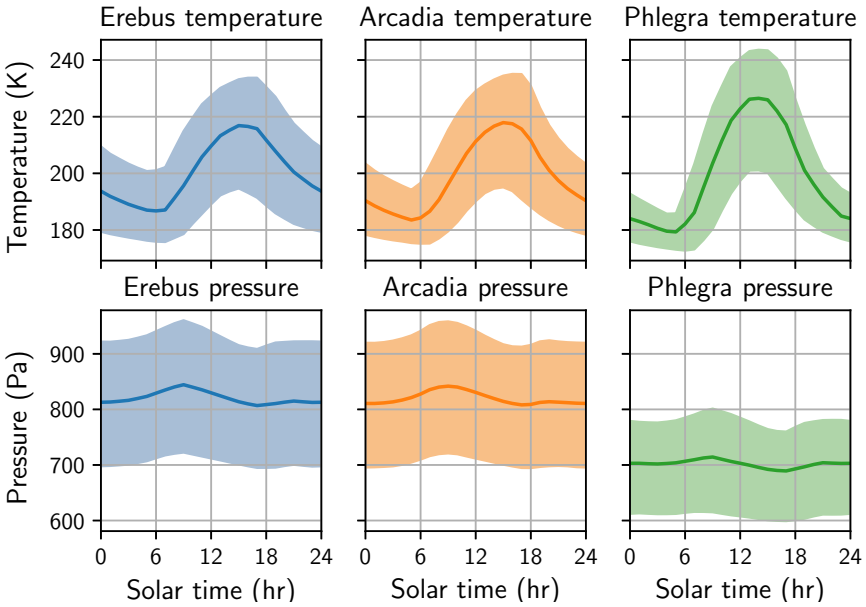

Figure 2.1: Variation in local temperatures and pressures at the three representative landing sites across a single local day, with maximum and minimum curves for one Martian year

This low pressure and temperature places the majority of the atmospheric resource acquisition system below the triple point of carbon dioxide (517 kPa, 216.6 K) - an unusual situation for a compressor. If the temperature of the gas falls below the sublimation line solid crystals will form in the gas stream. This is somewhat analagous to the formation of water droplets in a steam turbine dropping into the vapour dome. However, the formation of solids could reasonably be expected to be more destructive to the hardware of the acquisition system than droplets in a steam turbine, with rapid erosion and mechanical damage to any surface the gas flow impinges on. As such, it is important that the working line of the acquisition system is kept far from the sublimation line unless deposition is intended and adequate controls are put in place.

To find appropriate properties for the working gas of the atmospheric system, calculated properties for pure carbon dioxide were evaluated using CoolProp [26] across the compressor working envelope. The properties on the sublimation line were validated with data from Vukalovich [27], due to the importance of identifying and avoiding this region. Data from CoolProp was tabulated to allow for the rapid plotting of temperature-entropy diagrams with real gas properties. Single values of gas specific heat capacity and ratio of specific heats were calculated from an average across the working envelope, to be used in the rest of the design process.

2.3.1 Dust

In the literature, much is made of the impact of Martian dust on all surface systems - particularly on systems handling large volumes of atmospheric gases. Without the presence of water to clump and precipitate dust particles, they can reach sub-micron sizes and evade traditional removal techniques. The particularly fine Martian dust carried by the wind is commonly referred to as ‘fines’. However, the impact of this on a turbomachinery-based system is expected to be relatively minimal and can be mitigated with a number of simple approaches.

Rapp [20] reports a general agreement between sources on the properties of airborne fines, based on solar absorption analysis. The number-weighted average particle diameter is around 0.25 µm and a mass-weighted average of 2.5 µm [28] - considerably finer than talcum powder. The average number density in a 20 km atmospheric column was found to be 4.6×10^6 particles per square centimetre of ground area or 2.3 particles per cubic centimetre. Other methodologies

have found similar values for overall density, with only a small increase near the surface [29].

A particle density of 2.3 per cubic centimetre is equivalent to a dust density of 28 ng per cubic metre or 1.4 µg per kilogram of atmosphere. Based on the target flow rate, over the 500 day operating lifespan of the system, the expected ingested dust would be just 800 grams. Even when conservatively accounting for dust densities perhaps an order of magnitude higher than the column average this is a comparatively small quantity. However, it still must be appropriately removed from the gas stream.

To prevent fouling and abrasion of the atmospheric resource acquisition system, airborne fines must be removed from the gas stream as early in the machine as possible. Three alternative approaches may be suitable - cyclone separators, electrostatic precipitators and HEPA filters [30].

Cyclone separators operate by swirling air in a cylindrical cavity, such that dense particles migrate to the outside by centrifugal effects and are slowed by the boundary layer. Cyclones require high gas speeds (above 10 m/s) and have comparatively low pressure drops (around 10-20 times dynamic pressure), but are only suitable for extracting particles above a certain size threshold. This makes cyclone separators ideally suited for placement near the front of the system where densities are low and volumetric flows are high, where the majority of the mass of the airborne fines can be extracted [31]. A representative cyclone separator might be expected to remove over 75% of the dust mass in the airstream, but leave a large number of particles smaller than 1 µm.

Electrostatic precipitators use a series of close-spaced plates across which a voltage is applied. Fines in the air are charged by electrodes before entering the stream, such that they migrate towards the plates in the precipitator and are thus removed from the airstream. Electrostatic precipitators are functional with much smaller particle sizes than cyclone separators but require long, narrow flow passages to be effective - leading to comparatively high pressure drop. This makes them better suited to later stages of the machine where volumetric flow is lower [32]. Higher pressures also allow for higher voltages before electrostatic breakdown occurs, according to Paschen's law.

Finally, HEPA filters use many layers of fine-woven fabrics and meshes to trap particles. These are extremely effective down to practically any particle size but have the highest pressure drop of the three options and eventually clog with dust [21]. Because of this, and the relatively high density of effective filters, it is desirable to minimise the cross-sectional area of any fabric filters and to minimise the dust applied to them. Based on this, HEPA filters would be best applied as late in the machine as possible, protecting only the most dust-sensitive components.

Since no dust removal systems are perfect, the resistance of mechanical components to dust damage must be considered. As Martian fines are less numerous than equivalent atmospheric dust on Earth [33], the impact is expected to be less than on terrestrial compressors. While accommodations must be made for the increased blade roughness caused by slow dust erosion this is not expected to be a major issue for the majority of stages in the atmospheric resource system. A future work could more closely examine the integration of the dust mitigation system into the atmospheroc resource acquisition system.

With the ISRU system requirements and performance evaluation through the ESM framework, as well as the relevant properties of the Martian atmosphere, enough information has been gathered to begin the design process. The next section will detail the methodology used to design and optimise the atmospheric resource acquisition system.

3 Method

In order to access the most degrees of freedom while making the design task tractable, two 'levels' of analysis have been used. The top level is *architectural design*, which sets the overall parameters of the system such as mass flow and number of components, and the required performance of each component (compression ratio, heat removal, etc). The *component design* then uses a low-order model of the behaviour of each component type to determine the best geometry and flow parameters to meet the performance specified by the higher-level *architecture*. The components models have been verified and validated against literature and engineering expectation.

With this approach a wide design space has been mapped out, and an optimal design for the atmospheric resource acquisition system has been found for the assumptions and requirements used.

3.1 Architectural Design

Underpinning the optimal design of the atmospheric resource acquisition system is the choice of architecture - the choice of high-level parameters and of which components are placed where in the system. The architecture constrains the performance of the system, and defines the 'duty' around which each individual component must be itself optimised. In this work, 'duty' collectively refers to the pressure ratio of compressors and cooling power of heat exchangers, which are both specified at the *architectural* rather than *component*-level design.

The architectural design space is considerably more tractable than the design of each component, possessing just four quantitative high-level parameters (number of intercoolers, mass flow, intercooler outlet temperature and compressors per intercooler) plus compressor topology selection. The architectural design space also has clearer relationships between the choice of parameter values and expected system performance. The two most important of parameters (number of intercoolers and mass flow) were searched to find the combination that gave the highest performing design, with the other parameters held constant. Due to the relatively small number of combinations, an exhaustive search through these two parameters was used.

3.1.1 Quantitative Variables

The two most impactful architectural parameters open to designer control are the number of intercooling units, and the mass flow through the acquisition system. Due to their relatively high importance, these were the only two parameters used in the architectural design in this work. Other architectural parameters are the outlet temperature of the intercoolers, number of compressors between intercoolers, targeted system outlet pressure and the expected pressure drops and efficiencies of the intercoolers and compressors respectively. These last two can either be estimated, or determined directly through a component-level optimisation. Finally, the non-numerical parameters are the choices of compressor type used at each point in the system.

The number of intercoolers, as well as number of compressors between intercoolers and the intercooler outlet temperature, determine the inlet temperature and thus strongly influences the specific work of each compressor. The number of intercoolers is the freest variable of these - the intercooler outlet temperature is limited by the temperature of heat rejection from the radiators, and the number of compressors between intercooler is must be a low integer value.

The chosen mass flow indirectly determines the practical achievable efficiency of each compressor, mainly due to increasing passage sizing and reducing relative tip gaps in rotating components. A higher mass flow also leads to an increase in the mass of each component. An increased

Variable	Impact on power	Impact on mass
Number of intercoolers ↑↑	↓ More intercooling lowers average T_{in} for compressors	↑ Intercoolers add mass
Mass flow ↑↑	↑↑ Compressor efficiency increases slightly with higher volumetric flow	↑ Each component becomes slightly larger to pass more flow
Intercooler outlet temperature ↑↑	↑↑ Increases average T_{in} and thus work for compressors	↓ Mass of intercoolers decreases slightly with less cooling
Number of compressors between intercoolers ↑↑	*Uncertain* Decreasing pressure ratio of each stage changes efficiency, depending on optimal for the compressor type	↑ Lower pressure ratio compressors are not substantially lighter, and more are needed

Table 3.1: The qualitative variation of atmospheric resource acquisition system power consumption and mass with the increase of each of the four architectural variables

mass flow per second is achieved by running the acquisition system during certain portions of the day only and storing the carbon dioxide for use in a continuously-operating electrochemical process. This storage requires either a large tank for storing high-pressure gas, or a condensing heat exchanger and smaller tank for storing liquid.

The qualitative impact of each of the four quantitative architectural variables is shown in Table 3.1, with the expected impact of each on the whole system mass and power consumption and thus ESM. The impact on cooling power is not shown, as this is expected to closely correlate with power consumption.

With the selection of the high-level parameters for each design, much of the performance of the atmospheric resource acquisition system is already constrained. Most high-level parameters allow a trade-off between mass and power of the system. An understanding of the links between these parameters and system performance is thus essential for good design insight.

3.1.2 Compressor Topology Selection

As well as the quantitative architectural variables, a key choice at this stage is the type of compressor used at each point in the machine.

Three types of compressor have been considered in this work: axial, centrifugal and scroll. Axial and radial compressors are both dynamic compressors: in an axial compressor the spinning rotor and fixed stator are arranged in-line with mostly axial flow between them, in a radial compressor the spinning impeller turns the flow from mostly axial to mostly radial with the diffuser extending in the radial direction. In contrast, scroll compressors are positive displacement machines using moving interlocking spirals to force gas from a large to a small volume, increasing pressure.

The choice of optimal compressor type from the options of axial, centrifugal and scroll depends on many factors. Of these three, axial compressors have the highest efficiency and the lowest weight, but have the lowest achievable pressure rise across a single stage - around 1.3 in carbon dioxide based on common work coefficient limits for subsonic axial compressors. A very large number of stages would thus be needed, which would be extremely sensitive to inlet conditions

and may suffer from inefficiencies due to poor matching at design or off-design conditions. In contrast, scroll compressors are comparatively heavy and inefficient but can tolerate very high pressure rises. The MOXIE scroll compressor is a single-stage machine with a compression ratio of 110, but an isentropic efficiency of just 10%. Centrifugal compressors are intermediate to these two types with intermediate efficiency, weight and pressure rise. The achievable pressure rise for non-supersonic compressors (ie. those with reasonably high compression ratios and efficiencies) in carbon dioxide is around 2.35.

The efficiency of both axial and centrifugal compressors suffer at very small sizes and volumetric flow rates, due to tip gap leakage flows. This makes the dynamic compressors less suitable for low mass flows and high pressure compressors. In contrast, scroll compressors can pass almost arbitrarily low volumetric flows without a drop in efficiency due to mechanical sealing between moving and fixed elements.

Given these characteristics of each compressor, the selection for each component in the atmosphere acquisition system is a nontrivial problem, depending on the optimisation goals as expressed in terms of ESM. This choice largely exists as a tradeoff between efficiency (and thus power consumption and cooling) and mass of each compressor.

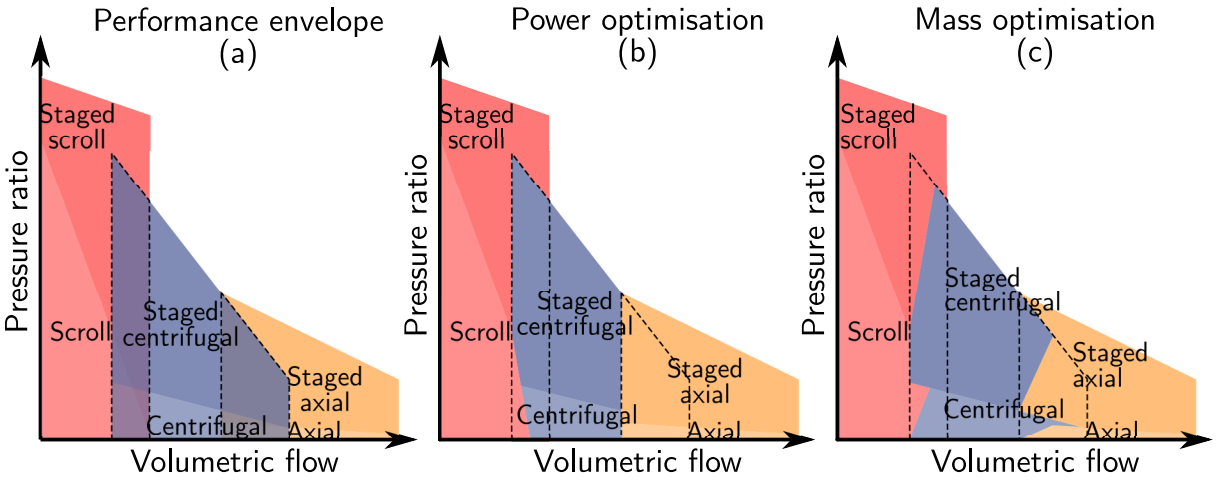

Figure 3.1: A set of schematic performances envelope for axial, centrifugal and scroll compressors individually and staged, on axes of pressure rise and volumetric flow. The region of overlap is marked with a dashed line. Reproduced and modified from [34]

This trade-off particularly around choice of compressor type is shown schematically in Figure 3.1 which plots the performance envelopes of the six alternatives for achieving a given compression ratio. For large regions of the overall envelope, the choice of compressor is comparatively easy as the alternatives would be impractical. However, for the overlapping regions, there are several viable options, with the best depending on the optimisation goal in question. Figure 3.1 (b) and (c) show the optimal choice if only power or only mass is the performance metric. In this, where Equivalent System Mass includes both mass and power with appropriate weightings, the optimal choice will depend on the exact value for each choice of compressor and so these regions will be less clearly divided. The framework ultimately used for topology selection in each component is direct comparison between alternatives at each point in the machine with the lowest ESM topology selected.

3.1.3 Architectural Design Implementation

The above high-level parameter and component topology choices can be used, with some simplifying assumptions, to implement a practical framework for architectural design of the atmospheric resource acquisition system.

The variables of intercooler number and mass flow were taken as the only architectural design variables for this study. As the daily mass acquisition for the system is an overall requirement, varying the mass flow involves the variation of the duty cycle of the acquisition system. Since this two-variable design space is substantially more tractable than the full multivariable space, it is possible to use a brute-force search approach rather than a full optimisation. A sweep through the appropriate mass flows and intercooler numbers can be carried out and an optimum manually found. The number of compressors between intercoolers is maintained at one, and the intercooler outlet temperature is held at 250 K.

The mass flow through the atmospheric system was varied by changing the hours of operation of the system as a whole - only operating for a few hours each day to increase mass flow per second while not exceeding the daily mass flow requirement. The values of mass flow used, along with supporting information on the relevant duty cycle are given in Table 3.2. Intercooler numbers of 10, 15, 20, 25 and 30 were used in the brute-force search.

Each of these intercooler numbers was tested with each mass flow, giving 25 designs generated. Once the best of these was found, alternatives with one more or one fewer intercoolers, and slightly higher and lower mass flow, were also tested. This allowed the optimum mass flow and intercooler number to be found with a minimal number of designs generated.

Mass flow (g/s)	Daily hours of operation	Liquefaction and storage?
11.3	24	✗
22.5	12	✓
33.8	8	✓
45.1	6	✓
90.2	3	✓

Table 3.2: Values of number of intercooler and mass flow, over which parameter sweeps are carried out. The associated duty cycle parameters associated with each mass flow are also given.

For each of the combinations of mass flow and intercooler number, the relevant system is designed with per-component machine optimisation. Each component's input flow properties are determined, the component is optimised for the relevant required compression or cooling, and the output flow properties are then calculated for use in the next component. In the scheme implemented, the first compression stages are hard-coded to be axial compressors to both take advantage of the low density intake gas and thus high volumetric flow rate, and to set up the high velocities required for a cyclone dust separator. After these stages, the default component sequence is alternating centrifugal compressors and intercooling heat exchangers. After the optimisation of each centrifugal compressor it is compared to an equivalent pressure ratio scroll compressor. If the latter has a lower Equivalent System Mass, the default compressor type onwards switches from centrifugal to scroll. Once the complete sequence of components has been calculated, the number of scroll compressors is optimised by re-analysing the machine with a varied number of compressors and finding the minimum ESM option. Finally, the system output pressure is checked against the target output. If there is a substantial mismatch, the system

optimisation is repeated with an adjusted pressure ratio target for all compressors.

The result of this architectural optimisation is a complete description of the atmospheric resource acquisition system, with each component optimised and the flow fully described.

Once each atmospheric system is generated, its performance was evaluated over an appropriate day (with data processed from Section 2.3). The speed and non-dimensional flow properties of compressors were assumed constant, and the efficiency and specific work of each component estimated using the Smyth and Miller method [35] . The total required energy is then summed across all hours of operation, and the maximum cooling power found. This allowed for the final calculation of power generation capacity, cooling capacity and energy storage required to operate the atmospheric resource acquisition system.

Two options exist for evaluating the performance of each system, both of which were used and compared. The ESM of the atmospheric system could be used in isolation, or found for the entire integrated propellant ISRU system with water extraction, electrochemical processing and propellant liquefaction. The latter requires more assumptions to be made, but would produce a more effective entire system. A very low-order model of the ISRU chemical processing system was developed through scaling of an existing system [19], with appropriate considerations for variations in the design of the atmospheric system. This included appropriate changes to the power consumption and cooling requirement with a liquid carbon dioxide inlet, where the enthalpy of carbon dioxide vapourisation can be used to reduce product stream liquefaction cooling demands [36].

This two-variable approach to architectural design provides all the necessary information for component-level optimisation, as well as a framework for evaluating the relative merit of the final system. It provides sufficient information for compressor topology optimisation to occur, without either increasing design system complexity or limiting designer choice. By using a brute-force search through the most important high-level parameters, the system behaviour can be well understood and an optimum design easily found.

3.2 Component Design

Once the architectural design has determined the required duty of a component, the design of that component can proceed. This involves an optimisation of the geometry and other parameters of the component to minimise Equivalent System Mass.

The four types of component specified by the architectural optimisation are axial, centrifugal and scroll compressors and intercooling heat exchangers. The three compressors each have a pressure ratio duty specified, while the heat exchanger instead has a specified cooling power duty. All four have their inlet mass flow, temperature and pressure provided, with the properties calculated from the performance of the previous component. Each component is fully described by a number of parameters that describe the geometry and properties of the component. These parameters are varied by the optimiser to create a higher-performing component. They are also sufficient to calculate the mass, power and cooling of component.

3.2.1 Component Optimisation Framework

As well as the key output variables, the component optimisation calculates a number of geometric dimensions for each component. This allows the implementation of both soft and hard geometry-based limits in the optimisation loop.

Two alternatives exist for component optimisation - per-component and whole-system optimisation. In the former, each component's descriptive parameters are optimised individually in

Axial compressor	Centrifugal compressor	Scroll compressor	Intercooling heat exchanger
Duty and input parameters			
Pressure ratio	Pressure ratio	Pressure ratio	Cooling power
Inlet flow ($\dot{m}$, p, T)	Inlet flow ($\dot{m}$, p, T)	Inlet flow ($\dot{m}$, p, T)	Inlet flow ($\dot{m}$, p, T)
			Inlet area
			Coolant-gas ΔT
Optimiser parameters			
Rotation speed	Rotation speed		Area expansion ratio
Flow coefficient	Flow coefficient		Tube pitch-diameter ratio
Work coefficient	Work coefficient		Coolant velocity
	Inlet hub radius		
	Diffusion ratio		
Output parameters for ESM calculation			
Mass	Mass	Mass	Mass
Efficiency	Efficiency	Efficiency	Pressure drop
			Coolant pumping power

Table 3.3: The input parameters for each of the components. The parameters in the first block are input by the architectural optimisation, the central descriptive block is subject to optimisation and those in the final block are output by the component model

sequence. This results in 20-50 separate optimisations each over 3-5 variables to produce a complete design. In the latter case, the entire system's descriptive parameters are optimised simultaneously with a calculation of inlet flows for each component at each step. This includes many more variables to optimise over (60-250) and a more complex calculation at each step of the optimiser - thus leading to a huge computational overhead.

The advantage of the simultaneous optimisation is it allows for co-optimisation of adjacent machines. For instance, the diffusion factor of centrifugal compressors and area expansion ratio of intercooling heat exchangers both control the amount of diffusion to slow the flow. When these are optimised simultaneously between an adjacent centrifugal compressor and intercooling heat exchanger, a better overall performance for these diffusing features might be obtained. Similarly, if a model for the driving electric motors was integrated into the design system, a co-optimisation of adjacent compressors sharing a common motor running at a single speed might allow larger, more efficient motors to be used.

However, the number of places where this manner of co-optimisation could deliver substantial gains is limited and the computational cost is high. Simultaneous optimisation was thus not used in this work.

The use of these descriptive parameters underpins the entire component optimisation process. Through the variation of just 3-5 variables and the appropriate component models the entire possible performance space can be accessed. The choice of per-component design makes an appropriate trade-off between optimisation speed and optimised system performance. This framework allows for rapid and effective design of optimal components with a suitable optimiser and low-order component models - the latter of which will now be laid out.

3.2.2 Component Models

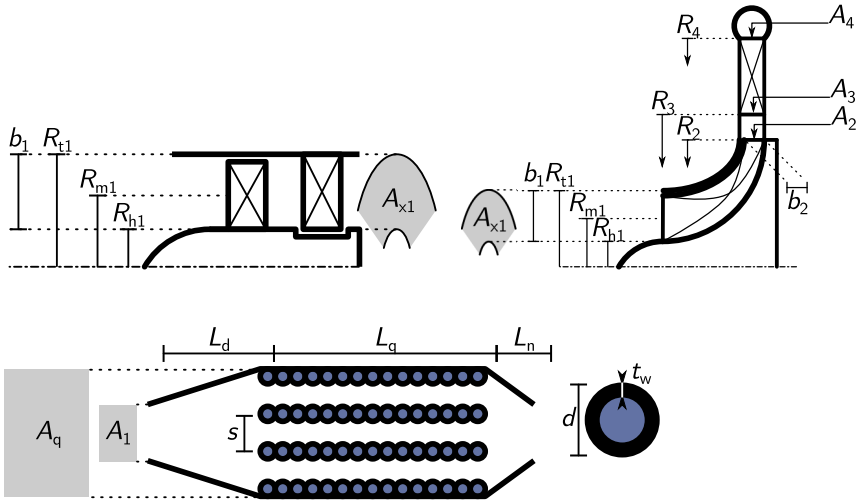

Figure 3.2: Component models for axial and centrifugal compressors, and intercooling heat exchangers, with key dimensions labelled

The component models used for the four analysed components - axial compressor, radial compressor, scroll compressor and intercooling heat exchanger - are detailed here. Each of these models were used to evaluate the performance of each component in the optimisation for the component. Diagrams with key dimensions labelled are shown in Figure 3.2, and the meaning of all symbols is listed in Appendix B. Swimlane diagram-style flowcharts showing the order of calculations of different variables are also shown for each component model.

Axial compressors are analysed using a relatively simple approach, with only work and flow coefficients and speed needed to determine relevant dimensions. The definition of flow coefficient Φ, when combined with speed, allows a calculation of inlet radius and area which immediately gives all radii. For the mass of axial compressors, an empirical correlation developed by Sagerser was used [38]. These equations are laid out in Table 3.4, with the meaning of each geometric dimension defined in Figure 3.2. The efficiency estimation for axial compressors is common with centrifugal compressors (both utilising a Smyth and Miller chart), and is detailed below. A swimlane diagram showing the interactions of the subsections of the axial component model is shown in Figure 3.3.

Parameter	Definition/Model	Units	Reference
Flow coefficient	$\Phi = \frac{V_x}{U} = \frac{V_x}{R_{m1}\Omega}$	-	[37]
Stage loading	$\Psi = \frac{\Delta h_0}{U^2} = \frac{\Delta h_0}{(R_{m1}\Omega)^2}$	-	[37]
Mass flow	$\dot{m} = \rho A_x V_x = \frac{p}{RT}(2\pi R_{m1} b_1) V_x$	kg/s	[37]
Weight	$W = 24.2(2R_{m1})^{2.2}\left(\frac{\Omega R_{t1}}{335}\right)^{0.5}\left(1 + \frac{0.434-0.218\frac{R_{h1}}{R_{t1}}}{0.281}\right)$	kg	[38]

Table 3.4: Model equations for axial compressor

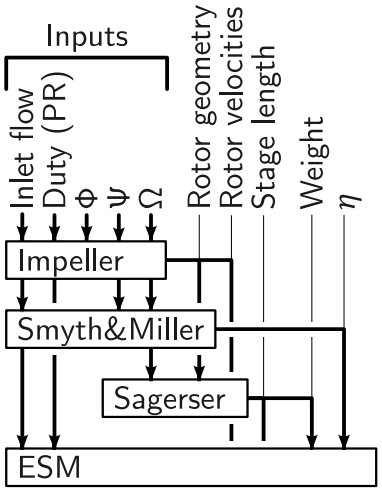

Figure 3.3: Swimlane diagram for calculation of different properties in the axial compressor component model

The analysis of the geometry of centrifugal compressors requires two additional variables to be defined, the inlet hub radius and diffusion ratio in the diffuser. The inlet tip radius is set to minimise relative inlet tip velocity, reducing losses. The impeller outlet conditions were fixed by assuming a pessimistic value for slip (σ) of 0.85, and setting radial velocity with the flow coefficient. Using this definition of flow coefficient simplified the analysis considerably. This approach has the benefit that it constrains the impeller exit metal angle, χ_2, and diffuser inlet flow angle, α_2, explicitly. The former of these can be used for CFD validation, the latter is used in the diffuser model. The relevant guiding equations are given below in Table 3.5.

Parameter	Definition/Model	Units	Reference
Inlet tip radius	$R_{t1} = \sqrt{2^{\frac{1}{3}} \left[\frac{\dot{m}}{\rho_1 \pi}\right]^{\frac{2}{3}} \Omega^{-\frac{2}{3}} + R_{h1}^2}$	m	[37]
Stage loading	$\Psi = \frac{\Delta h_0}{U^2} = \frac{\Delta h_0}{(R_2\Omega)^2}$	-	[37]
Impeller radial velocity	$V_{2,r} = U_2\Phi = R_2\Omega\Phi$	m/s	[37]
Impeller exit flow angle	$\tan\alpha_2 = \sigma\left(\frac{1}{\Phi} + \tan\chi_2\right)$	°	[37]
Impeller metal angle	$\tan\chi_2 = \frac{\frac{\Psi}{\sigma}-1}{\Phi}$	°	[37]

Table 3.5: Model equations for centrifugal compressor

The centrifugal compressor diffuser is modelled as a constant-angle logarithmic spiral with an optimal diffusion angle of 8 °(as determined from Figure 3.4a). The minimum-length maximum-efficiency points were recorded for each area ratio and a curve fitted through them, as is shown in Figure 3.4b. The diffuser area ratio, a descriptive variable in the component model, sets the area ratio between inlet and outlet and thus radius ratio. Length ratio is defined as the ratio of

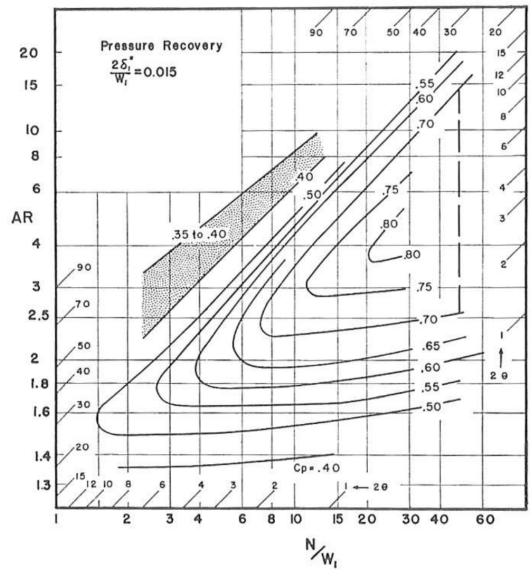

(a) Rectangular diffuser performance map[39], used as an approximation for diffuser performance in centrifugal compressors.

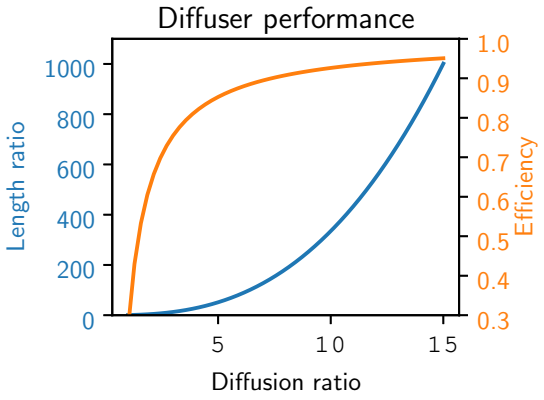

(b) Diffuser performance graph used in centrifugal compressor model

Figure 3.4

diffuser length to throat width, which could be used to find the required number of blades in the diffuser for optimal performance. However, such an analysis would likely require an accounting for flow blockage due to both boundary layer growth and finite blade thickness, so is beyond the scope of this model.

No reasonable centrifugal compressor weight model was found in the literature, so an explicit model based on geometry was used instead. This assumed a solid impeller and a 5 mm thick casing, with the volume and surface area respectively found with Pappus' Centroid Thereoms. The hub, tip and mean lines were all assumed to be circular arcs, with radii found from R_{h1}, R_{t1} and R_{m1}. The entire construction was assumed to be aluminium (which is suitable due to low temperatures throughout) although carbon fibre could also be used for reduced weight.

The efficiency of both axial and centrifugal compressors was estimated from the charts given by Smyth and Miller [35] to determine impeller efficiency from the flow and work coefficient of a generalised compressor. The contours of impeller efficiency for axial and centrifugal, shown in Figure 3.6a, were approximated with skewed ellipses of appropriate size, and thus allowed impeller efficiency to be quickly calculated for a given design. These elliptical approximations are shown in Figure 3.6b. As described by Smyth and Miller, these contours are deformed horizontally and vertically based on certain area and radius ratios of the compressor being analysed. Centrifugal compressor impeller efficiency is then further modified to account for tip gap, Reynolds number and Mach number with correlations from Casey and Robinson [40]. These modifications are given in Table 3.6, with Reynolds number and Mach number corrections acting on polytropic rather than isentropic efficiency.

Axial compressor diffuser (stator) efficiency is assumed to be equal to the impeller (rotor) efficiency. Centrifugal compressor diffuser efficiency is found from the curve-fit in Figure 3.4b. A flat 15% penalty was applied to diffuser efficiency to more closely match CFD validation, although this value could be altered based on a more comprehensive analysis in future work.

The overall centrifugal compressor model is shown schematically with a swimlane chart in Figure 3.5. This makes clear that the two additional degrees of freedom, the inlet hub radius and

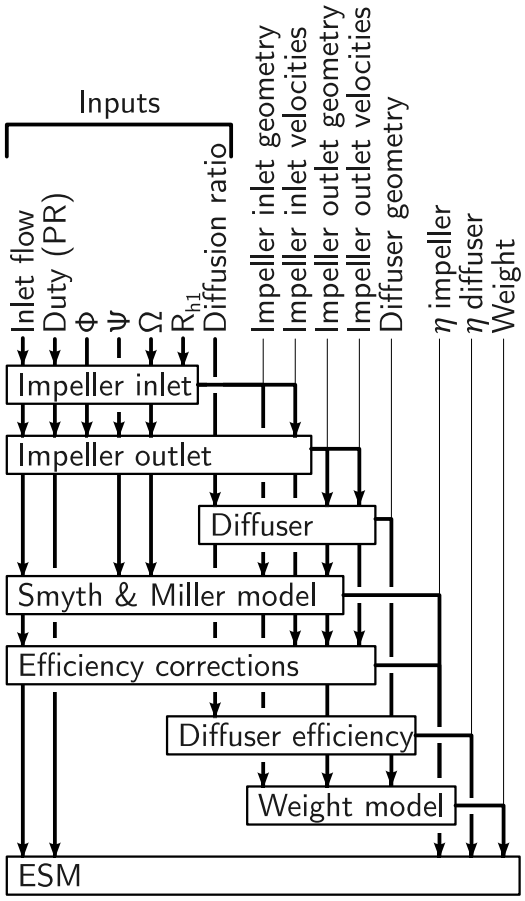

Figure 3.5: Swimlane diagram for calculation of different properties in the centrifugal compressor model

diffusion ratio, are needed to constrain the additional complexity compared to the axial compressor model.

The weight and efficiency of scroll compressors was not considered open to optimisation. In-

Parameter	Definition/Model	Units	Reference
Reynolds number parameter	$K_{\text{Reynolds}} = 0.05 + \frac{0.002}{\frac{\dot{m}}{4\rho_1 R_2^3 \Omega} + 0.0025}$	-	[40]
Reynolds number efficiency	$\Delta\eta_{\text{poly,Reynolds}} = -K_{\text{Reynolds}} \frac{1.5\times10^5 - \text{Re}_{\text{inlet}}}{1.5\times10^5}$	-	[40]
Mach number parameter	$X_{\text{Mach}} = \frac{\dot{m}}{4\rho_1 R_2^3 \Omega} \left(M_{2,\theta} - 0.8\right)$	-	[40]
Mach number efficiency	$\Delta\eta_{\text{poly,Mach}} = -0.05 X_{\text{Mach}}^2 - 3 X_{\text{Mach}}^4$	-	[40]
Tip gap efficiency correction	$\Delta\eta_{\text{tipgap}} = -0.003 \frac{\Delta b_{\text{gap}}}{b_2}$	-	[40]

Table 3.6: Efficiency corrections for centrifugal compressors with Reynolds number, Mach number and tip gap from [40]

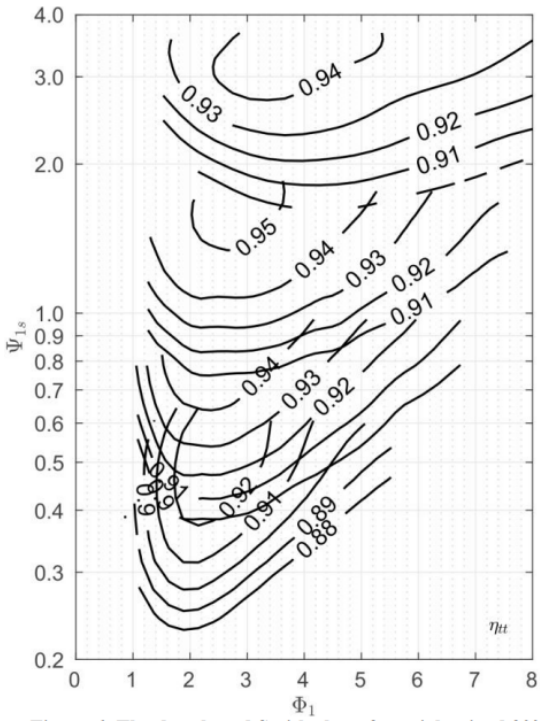

(a) Impeller efficiency plots from Smyth and Miller[35], in non-dimensional flow coefficient-work coefficient space. The bottom and top set of contours correspond to axial and centrifugal compressors respectively

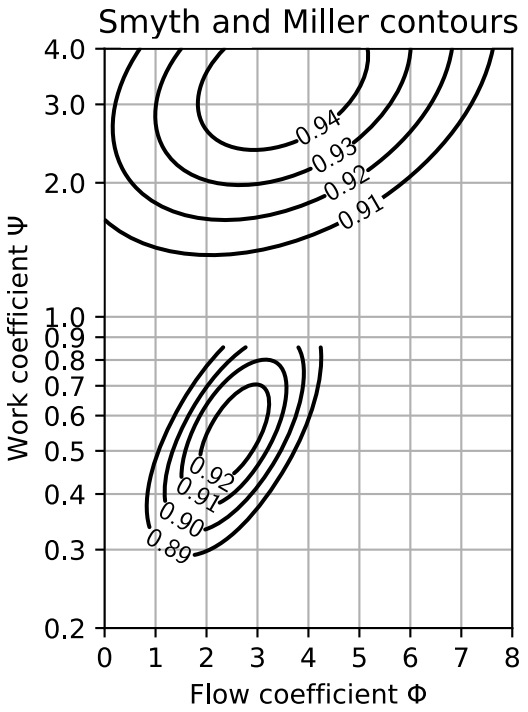

(b) Elliptical efficiency contours, extracted from Figure 3.6a and simplified to allow for faster calculation

Figure 3.6: Efficiency prediction methods for impellers of axial and centrifugal compressors

stead, following the work of Hinterman [21], the mass is scaled relative to volumetric flow to reflect the physical size of the hardware. Based on a literature review of commercial and research scroll compressors, a correlation for scroll compressor polytropic efficiency from pressure ratio was used. The mass and efficiency correlations are given in Table 3.7, with the survey of scroll compressor polytropic efficiency is shown in Figure 3.7. A swimlane chart showing the scroll compressor model is in Figure 3.8.

Parameter	Definition/Model	Units	Reference
Polytropic efficiency	$\eta_{\text{poly}} = 0.758 - 0.195 \log_{10}(\text{Pressure ratio})$	-	-
Weight	$W = 28.2 \left(\frac{\dot{m}}{0.03953 \rho_1} \right)^{0.8}$	kg	[21]

Table 3.7: Model equations for scroll compressor

The geometry of intercooling heat exchangers was calculated assuming a geometry with multiple 'walls' along the flow path, each composing of thin-walled tubes. With appropriate routing of coolant this creates a counterflow heat exchanger with high heat transfer and low pressure drop. This is similar to the technology pioneered by Reaction Engines for air-breathing engine precoolers [44]. Table 3.8 lists the heat exchanger model equations. The use of a channel geometry allowed the use of Haaland's relationship and an inverse Reynolds number scaling for turbulent and laminar flow respectively [45]. All of these use a hydraulic diameter, D_{h}, for Reynolds number, and a roughness, ϵ, to model the bumpy surface between brazed tubes.

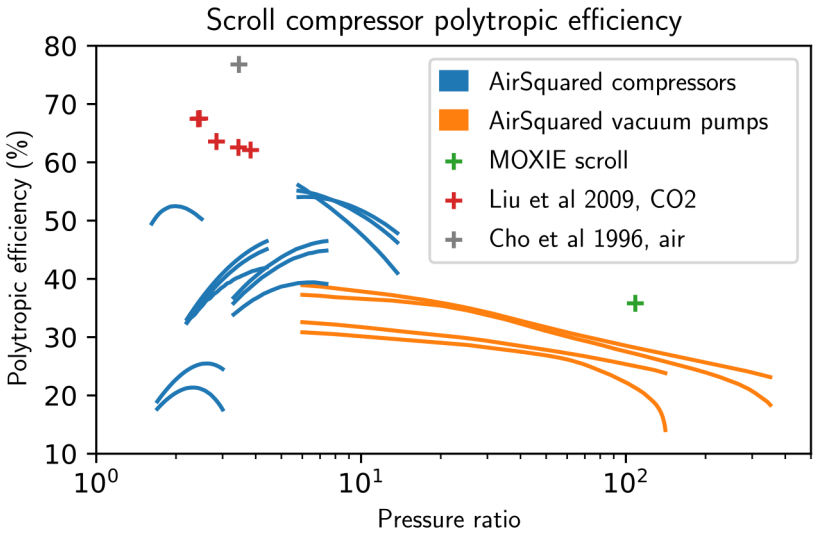

Figure 3.7: Literature review of seven commercial and three research scroll compressor polytropic efficiencies at a range of operating points, used to create the correlation in Table Equation 3.7. Data from [12, 41–43]

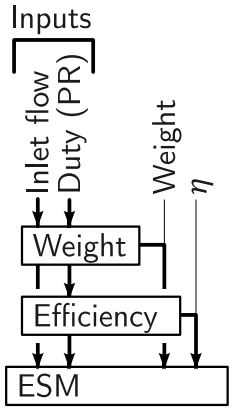

Figure 3.8: Swimlane diagram for calculation of different properties in the scroll compressor model

This friction factor can then be used in either the Chilton-Coburn relationship (fully turbulent flow) or Gnielinski relationship (low Reynolds number turbulent flow) to determine Nusselt number and thus heat transfer coefficient on the gas side. When Reynolds number is too low for turbulent flow, a constant Nusselt number is instead used. An identical treatment is applied to the liquid side of the heat exchange tubes, thus allowing for the overall heat transfer coefficient to be determined and the required area for heat transfer calculated. This required area gives both the heat exchange channel length and thus gas side pressure drop. The pressure drop calculation also includes terms for diffuser and nozzle pressure drops, set as 15% and 5% of the respective inlet dynamic pressures. The former of these was found from inspection of the plain rectangular diffuser map [39], the latter from traditional contracting section rules of thumb [46].

The weight model for the intercooling heat exchanger is explicit, summing the volumes of the heat exchange tubes and duct walls as well as diffuser and nozzle walls. A complete overview of the different interacting elements of the heat exchanger model is shown in Figure 3.9. Unlike the compressor models, there is much less forward dependency between model results. The majority of calculations operate on the descriptive parameters and initial inputs, or use very few results

from previous calculations. This reflects the physical relationship between the heat transfer and pressure drop in a heat exchanger channel (both are related to boundary layer profile).

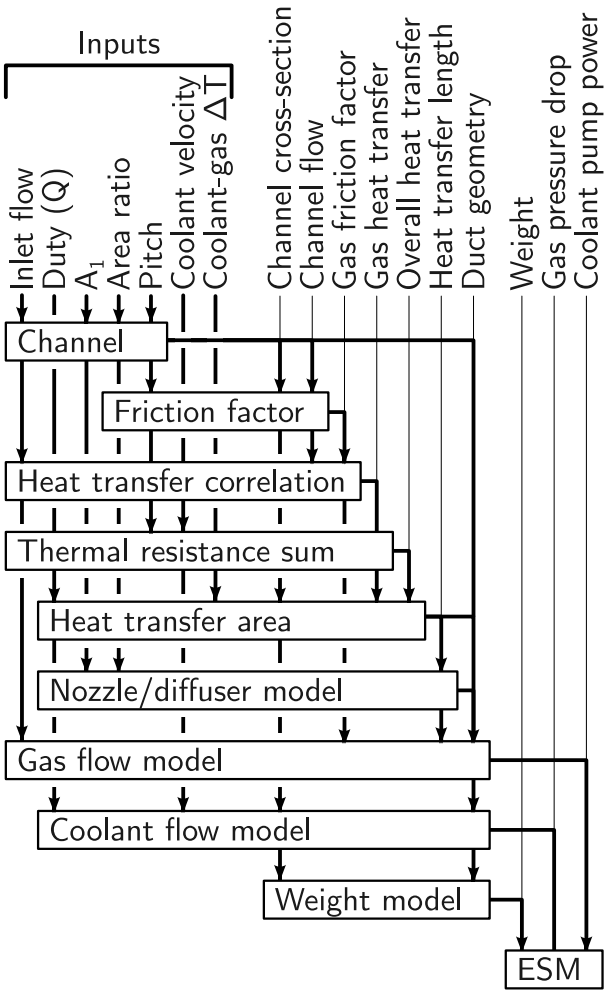

Figure 3.9: Swimlane diagram for calculation of different properties in the intercooling heat exchanger model

In summary, these four models allow the performance of each component from the relevant input parameters can be estimated. This then allows for optimisation of the model input parameters to minimise Equivalent System Mass of the component. The implementation of the component models with an optimiser is discussed next.

Parameter	Definition/Model	Units	Reference
Laminar friction	$f_{\text{laminar}} = \frac{64}{\text{Re}}$	-	[45]
Turbulent friction	$f_{\text{turbulent}} = \frac{1}{-1.8 \ln\left(\frac{6.9}{\text{Re}} + \frac{\epsilon}{3.7 D_h}^{1.11}\right)}^2$	-	[45]
Friction factor	$f = \begin{cases} f_{\text{laminar}} & \text{if Re} < 2100 \\ \max\left(f_{\text{laminar}}, f_{\text{turbulent}}\right) & \text{if Re} < 1 \times 10^4 \\ f_{\text{turbulent}}, & \text{if Re} < 4 \times 10^8 \end{cases}$	-	[45]
Nusselt number	$\text{Nu} = \begin{cases} 8.24 & \text{if Re} < 2300 \\ \dfrac{\frac{f}{8}(\text{Re} - 1000)\text{Pr}}{1 + 12.7\sqrt{\frac{f}{8}}\left(\text{Pr}^{2/3} - 1\right)} & \text{if Re} < 5 \times 10^6 \\ 0.125 f \text{RePr}^{1/3}, & \text{otherwise} \end{cases}$	-	[45]
Peak velocity	$V_{\text{peak}} = \frac{\dot{m}}{\rho A_2} \frac{s-d}{s}$	m/s	-
Pressure drop	$\Delta p = \Delta p_{\text{d}} + \Delta p_{\text{h}} + \Delta p_{\text{n}}$ $= 0.15\left(\frac{1}{2}\rho V_1^2\right) + \frac{L_{\text{h}}}{D_h} f \left(\frac{1}{2}\rho V_{\text{peak}}^2\right) + 0.05\left(\frac{1}{2}\rho_2 V_{\text{peak}}^2\right)$	Pa	[39, 45, 46]

Table 3.8: Model equations for heat exchanger

3.2.3 Component Optimiser Implementation

Using the descriptive variables and the geometric, weight and efficiency models described above, an optimiser can be implemented to find the descriptive variables that produce the best-performing component

As shown in Table 3.3, each component of the atmospheric resource system is described by a number of parameters input by the architectural optimisation, and a number of descriptive parameters subject to optimisation. The role of the component optimiser is to find the parameters that minimise Equivalent System Mass within the search space. The optimiser uses a Nelder-Mead method [47] (or downhill simplex method) to traverse the search space, with both soft and hard constraints applied to keep the produced components within sensible limits.

The Nelder-Mead algorithm is a heuristic optimiser approach that seeks the local minimum of a cost function in a multidimensional parameter space. For the optimisation of a function with N inputs, it evaluates the function on each of $N + 1$ points in a simplex - the N-dimensional equivalent of a tetrahedron in 3D space. Based on the values of the cost function at each point, the simplex is deformed and the process repeated. This continues until the simplex has converged onto a local minimum. If the function is comparatively smooth and the starting simplex appropriately bounds the expected minimum, this local minimum will closely match the global minimum. The choice of the starting simplex is thus an important one to allow both quick and effective optimisation.

For the scroll compressor, no parameters are available for optimisation, as the model for efficiency and weight is a simple scaling of existing hardware. For both the axial and centrifugal compressors, an initial guess for each parameter is calculated using specific speed and specific diameter arguments, and an upper bound guess is found from reasonable design limits. The starting simplex is then drawn between the upper bound guess and a scaled initial guess - thus encompassing the majority of the search space. The intercooling heat exchanger does not have an analogous construct to specific speed/diameter, and so reasonable upper and lower limits for each parameter are used to build the starting simplex. A narrower starting simplex would lead to faster convergence but may miss the global optimum value.

For each optimised components, hard and soft limits were imposed to keep the component physically plausible. These were imposed both onto the Nelder-Mead algorithm (with hard bounds that clipped any deformation that would extend the simplex beyond the limits) and through penalties to the ESM cost function. The latter of these are applied through a quadratically-increasing mass penalty when a parameter - either input or calculated - passes a soft limit. The magnitude of this penalty was hand-tuned to an appropriate value.

An example of this is shown in Figure 3.10. The two geometric limits imposed, bladeheight and hub radius, each cause the ESM as evaluated by the solver to jump above the 'true' ESM which the compressor would actually possess.

This approach for optimisation works well for axial and centrifugal compressors, where all output parameters (mass, efficiency) can be converted easily to an Equivalent System Mass basis. Some additional nuance is needed for intercooling heat exchanger pressure drop. The conversion from pressure drop to ESM is not simple and is likely highly variable with different architectural parameters.

The optimisation of intercooling heat exchangers proceeds as follows. A target pressure drop of 5% of inlet dynamic pressure is set, with a soft ESM penalty imposed if the evaluated heat

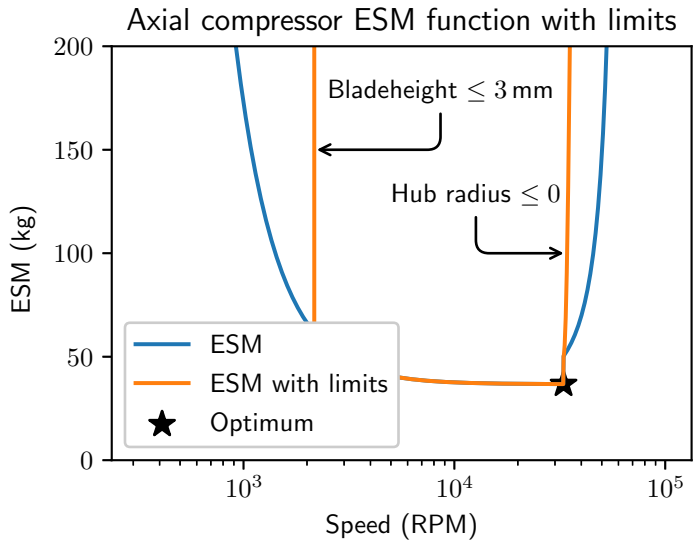

Figure 3.10: The Equivalent System Mass of an axial compressor evaluated by the optimiser function, as rotational speed varies.

exchanger has a pressure drop greater than this. The optimisation then proceeds using Nelder-Mead. If the final heat exchanger produced by the optimiser has a pressure drop greater than this target it is rejected, the target pressure drop is increased by a factor of 20% and the process is repeated. This approach is not computationally optimal, as several optimisation passes may be required, but it reliably produces low pressure drop designs with reasonable physical limits. This was not the case for other optimisation approaches trialled, including the use of models for ESM equivalencies of pressure drop. The effect of pressure drop on ESM is not constant throughout the machine, with a magnitude depending on the overall machine performance characteristics. This magnitude is not known a priori, so attempts to approximate it lead to poor results and either extremely high or extremely low pressure drops claimed to be optimal.

All four of these component optimisers are implemented in Python, with the `scipy` module's implementation of the Nelder-Mead algorithm. All component models were implemented in an object-oriented style to allow for easy extension and modification. The complete code is available online in open-source [48].

3.2.4 Component Model Validation and Verification

Before proceeding with further analysis, it is necessary to confirm that the component models are reasonable. This requires both validation (confirmation that the model matches real data) and verification (confirmation that the model behaviour is as expected).

Validation was carried out by comparing the geometry and performance predictions of each model to examples from literature. Four axial compressors [49, 50], three centrifugal compressors [51–53] and two heat exchangers working at eight operating points [54, 55] were found with appropriate data availability. Efficiency and key geometric properties were extracted from each compressor, and pressure drop and heat transfer were extracted from each heat exchanger operating point. None of the cases found included a validation of the component weight, due to the rarity of weight being a primary design driver. The results of the comparison between these literature results and the results produce by the component models is given in Figure 3.11.

The errors for both geometric properties and efficiency of axial compressors are relatively small with tight ranges, indicating the model is performing well. The largest error range is for hub radius, which may reflect the design of blades that shorten across their chord. Geometries were

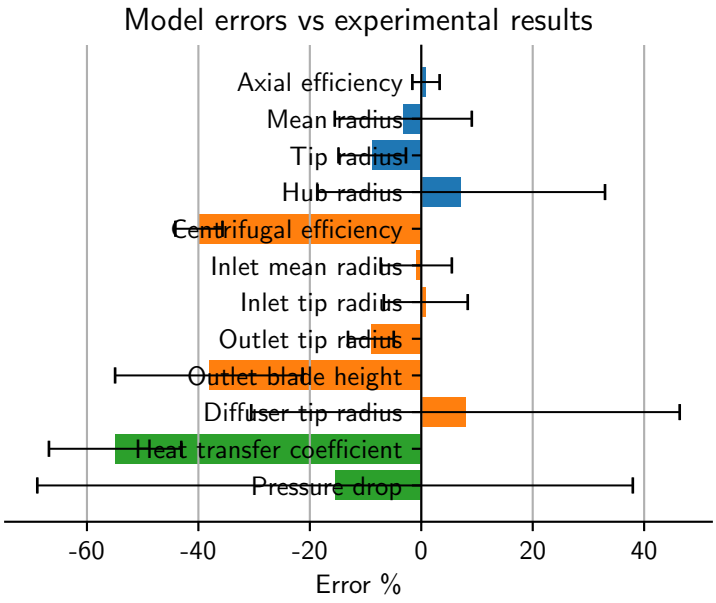

Figure 3.11: Error between experimental results from [49–55] and values predicted by each component model

measured at inlet so some error may be introduced here.

Centrifugal compressor inlet geometry is predicted relatively well, although both outlet blade span and diffuser outlet radius show large errors and wide error ranges. The former of these is likely due to the reduction in flow area caused by finite-thickness blades (not considered in the model as it introduces additional degrees of freedom) and the latter because the model only considers a logarithmic spiral, unlike the mixture of curved blades and straight wedges used in the test cases. Centrifugal efficiency is dramatically under-predicted by the model, by as much as 37 percentage points. This is likely due to a combination of pessimistic model assumptions on diffuser efficiency, the underestimation of impeller outlet blade span causing an excessive tip leakage correction, and the degree of efficiency optimisation possible for centrifugal compressors. If such an improvement could be achieved for the centrifugal compressors in the atmospheric resource acquisition system it would dramatically improve overall performance.

The intercooling heat exchanger model does not accurately predict either heat transfer coefficient or pressure drop. This suggests the underlying correlations used in the model are not accurate to reality - due to considerations such as turbulence introduced by the driving fan, intake effects, nonuniform flow or the effects of surface roughness. Interestingly, the model under-predicts pressure drop in a flat-plate heat exchanger [54] but over-predicts for a corrugated heat transfer surface [55] that likely more closely matches the actual brazed-tube geometry - showing that higher order effects are playing a significant role. Since the model seems to under-predict heat transfer, practical heat exchangers may be smaller and lighter than those produced by the optimiser.

Verification was carried out by checking that changes in model input produced changes in output that matched engineering expectation. For each component type, an certain optimal design was generated along with a number of suboptimal ones with different input parameters. These are visualised in Figures 3.12, 3.13 and 3.14. As the input parameters of each input model are varied, the component performance and geometry evolves in the expected way - thus verifying that they are capturing the correct behaviour. Contour plots of various performance metrics have

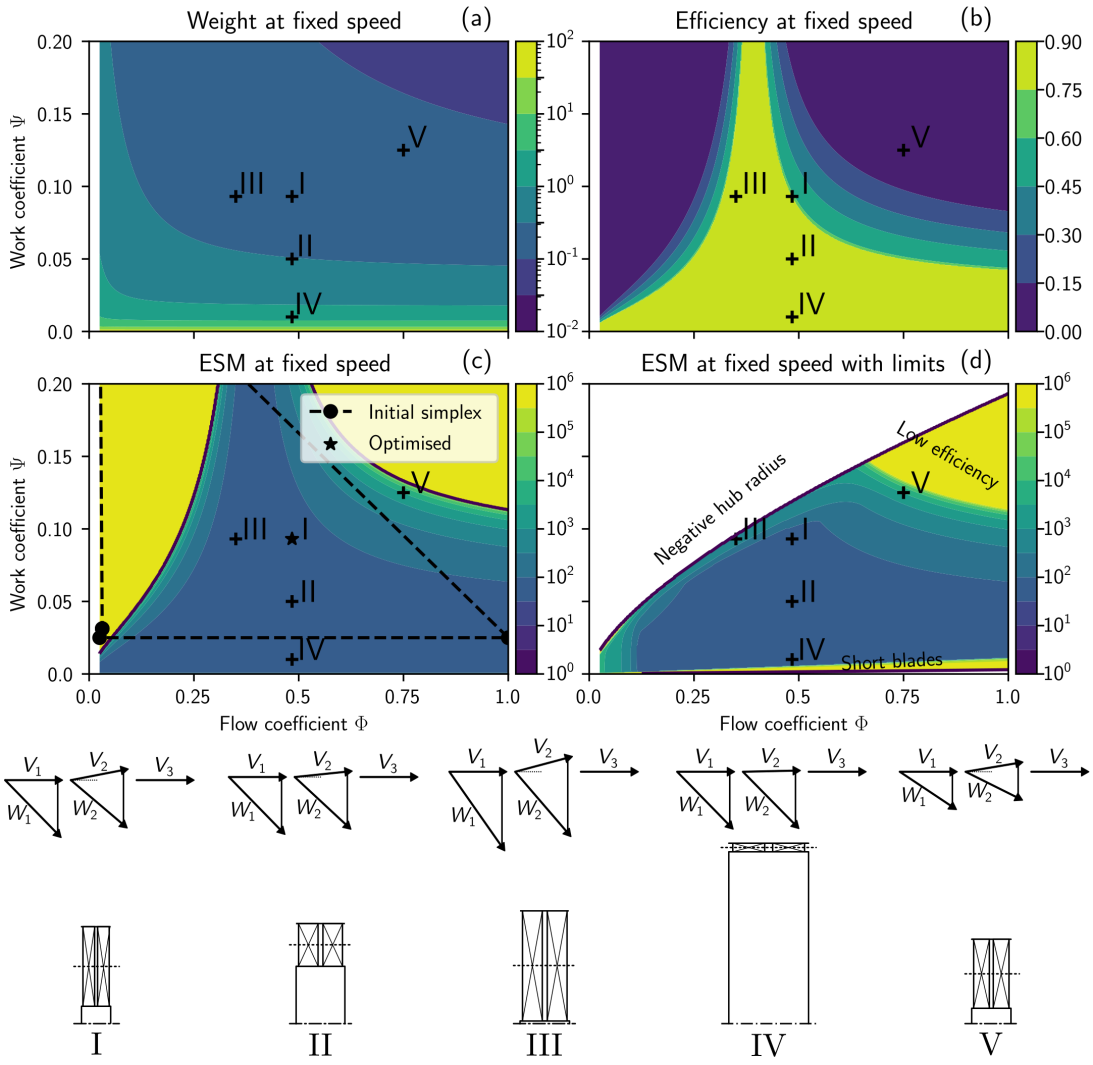

Figure 3.12: Axial compressor design maps, with pressure ratio 1.1 and inlet pressure 1.2 kPa

been generated to help visualise the model's prediction of the merit of each of these suboptimal designs. The Nelder-Mead starting simplex is also shown.

This analysis for axial compressors is presented in Figure 3.12. Plots of predicted weight and efficiency in flow coefficient-work coefficient space are shown, along with the combined Equivalent System Mass with and without the constraints added by the optimiser model. Rotational speed was held constant at the same value as the optimum in all cases. The optimised design, **I**, fits in the high-efficiency region with high flow coefficient (reducing the required flow area) but below the efficiency drop-off, and with high work coefficient but reasonable hub radius. Reducing work coefficient as in cases **II** and **IV** increases mean radius and thus reduces bladeheight, as expected. Reducing flow coefficient, as with case **III**, increases flow area until the hub radius reduces to a small value which is penalised by the optimiser. Increasing work coefficient in Case **IV** would reduce mass slightly due to slight diameter reduction but also causes excessive velocities that result in high frictional losses.

Similarly, the intercooling heat exchanger model was examined, with results shown in Figure 3.13. All designs use the same coolant inlet properties, inlet area and cooling power. The optimal case **I** has an intermediate diffusion ratio to reduce flow speed, and a short heat exchange section, both reducing overall pressure drop. Case **II** uses a larger heat exchange tube pitch which needs a much longer heat exchange section and a much greater weight. Case **III** has a larger diffusion

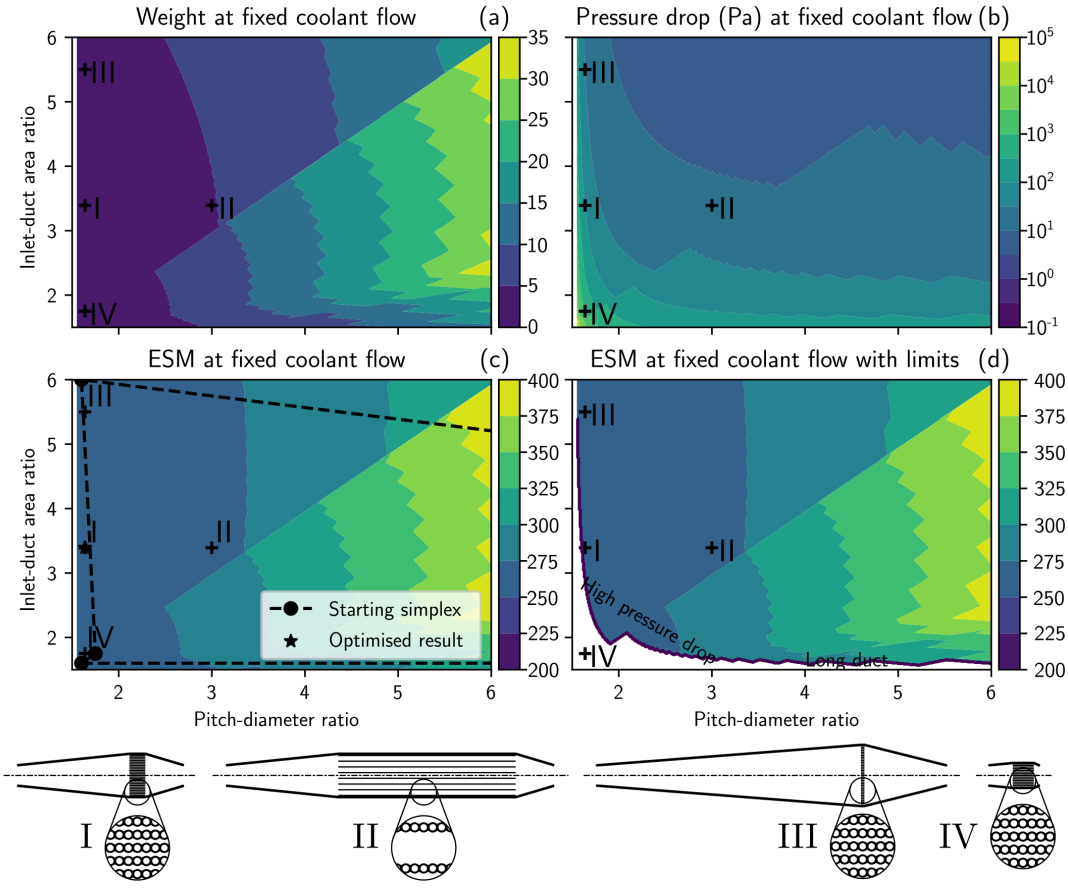

Figure 3.13: Heat exchanger design maps, with cooling power 1.75 kW and inlet pressure 45 kPa

ratio, a very short heat exchange section due to the large number of wide channels, a higher weight but a larger required coolant pumping power. Case **IV** uses a very low diffusion ratio, and thus a high flow speed in the channels and an unacceptably high pressure drop.

Finally, six centrifugal compressors were analysed, and are shown with contour plots and schematic impeller drawings in Figure 3.14. Due to the additional degrees of freedom of the centrifugal compressor model, plots of performance are shown on both flow coefficient-work coefficient space, and diffusion ratio-speed space. Inlet hub velocity was held constant for all cases. The optimal design **I** operates at the maximum allowable work coefficient and speed to reduce impeller size, and a reasonably low flow coefficient to keep impeller outlet blade span large. Reducing work coefficient in **II** increases impeller diameter and thus weight, and increases wetted area to reduce efficiency. Increasing the flow coefficient in **III** causes impeller exit radial velocity to increase, exit blade span to decrease and thus efficiency penalty from tip clearance leakage to increase. Varying diffusion ratio in **IV** and **V** directly trades off efficiency (due to better pressure recovery) with weight from increased diffuser size. Reducing speed while maintaining work coefficient, as in case **VI**, requires a substantial increase in impeller radius to maintain blade speed, causing a similar drop in performance as in case **II**.

Based on these validation and verification steps, it can be concluded that all component models are behaving as intended, and the optimiser is producing sensible results. Errors between the models and physical data are either small, or come from reasonable sources that are not captured by the low-order models used. Perturbations of optimised values are sub-optimal in physically reasonable ways, which further supports confidence that the model is capturing the broad strokes of the performance maps of axial and radial compressors and intercooling heat exchangers.

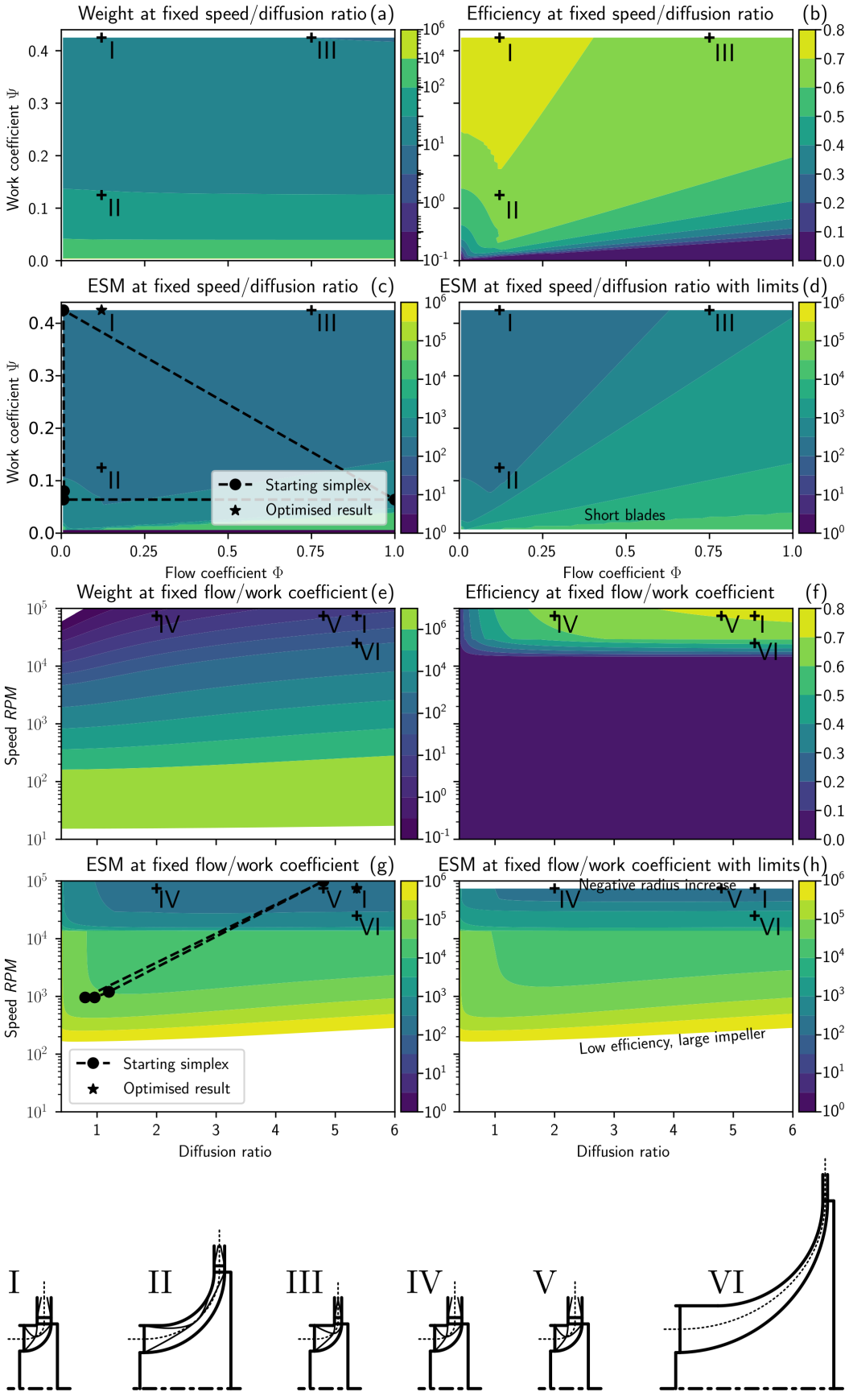

Figure 3.14: Centrifugal compressor design maps, with pressure ratio 1.5 and inlet pressure 30 kPa

3.2.5 CFD Validation

To further validate the turbomachinery efficiency models used and explore the underprediction of efficiency compared to literature, CFD of optimised compressors was carried out using the TBLOCK code. This is an especially important step given how foreign the operating regime is compared to standard turbomachinery analysis, and so existing correlations and models may become less accurate.

TBLOCK is a multiblock CFD solver specialised in solving flows in turbomachinery [56]. TBLOCK is written in FORTRAN77 and can be run on parallel CPU cores, allowing for very rapid calculation with simple geometries. It uses a structured hexahedron mesh and a single-step explicit solver to maximise speed at the expense of higher artificial viscosity requirements. All setup was carried out using a Python code to generate TBLOCK mesh files from template geometries [57]. A specific meshing code implementation was written to quickly generate centrifugal compressor rotors and diffusers based on the geometric parameters output by the component model, with the diffuser model implemented for this project.

Two centrifugal compressor designs - the first and last for the machine design determined as optimal - were each modelled in TBLOCK using a relatively coarse design mesh, and the isentropic efficiency calculated. This calculation assumed constant properties for gas properties (specific heats and their ratios), with values taken from the middle of the expected temperature-pressure range of atmospheric system. The values of these properties were found to be relatively constant away from the sublimation line. The calculated efficiency was then compared to the efficiency predicted by the component model. To test the effectiveness of the optimisation using the component model, various geometry parameters for the compressor were perturbed from their optimised values and the efficiency of each modified design calculated. If the optimiser (and thus, efficiency model) were working as intended, the efficiency should be maximum at the nominally optimal design, and be reduced slightly for each modified design.

4 Optimisation Results and Discussion

The methodology described above was used to produce an atmospheric resource acquisition system with minimum Equivalent System Mass. Designs were optimised both in isolation and coupled to the remainder of the in-situ resource utilisation system (using the approach described in Section 3.1). The latter of these is considered the overall optimum and is discussed below. The performance of the optimum system, and a comparison to an approximate cryofreezer system representative of current technology, is presented in Table 4.1. All atmospheric systems presented here use the default parameters for high-level parameters apart from mass flow and number of intercoolers - one compressor between each intercooler and a 250 K intercooler outlet temperature.

This section will present an overview of the optimised system and the improvements made to the ISRU plant as a whole by considering the integration with the atmospheric system, versus what would have been the result of ignoring integration. A justification of the results of the architectural design will then be shown, to demonstrate that the number of intercoolers and mass flow chosen is optimum. The component optimiser will be briefly discussed, with the results of the CFD validation of efficiency.

4.1 Optimised System

Variable	Design value	Service requirement	ESM	Approximate cryofreezer	Cryofreezer [14] ESM
Mass	267.4 kg	267.4 kg	267 kg	2500 kg	2500 kg
Power	11.36 kW_e	9.99 kW_e	1489 kg	50 kW_e	7450 kg
Cooling	18.26 kW_{th}	19.09 kW_{th}	2310 kg	50 kW_{th}	6050 kg
Energy storage	-	119.9 kW h	600 kg	600 kW h	3000 kg
Total			**4666** kg		**19000** kg

Table 4.1: The ESM of the optimised atmospheric resource acquisition system, compared to a generic cryofreezer equivalent

The optimum system, when considering the interactions with the ISRU stack as a whole, is one which operates for 12 hours during the night only and liquefies carbon dioxide for storage. The determined optimal compressor number was six axial compressors, eight centrifugal compressors and seven scroll compressors - the latter 15 all having a pressure ratio of 1.502, and having intercooling heat exchangers between each one. This provides an appropriate balance between mass, efficiency and compressor geometry for each component.

The temperature-entropy diagram of the optimised system process is shown in Figure 4.1. It is plotted with real gas properties for carbon dioxide, which were calculated using the process described in Section 2.3. As is visible, almost all compressors regardless of scroll or centrifugal have the approximate same efficiency. This reflects the fact that the optimiser switches from centrifugal to scroll almost immediately as the latter becomes more efficient than the former.

A breakdown of the optimised system's mass, power and cooling at a nominal operating point (an average of the conditions experienced during an average operating night) is presented in Table 4.2. As is expected, the axial compressors and heat exchangers each contribute a relatively small amount to the hardware mass due to their small size and the use of advanced thin-walled heat exchange tubes. The vast majority (over 95%) of the ESM of the atmospheric system comes from power, cooling and energy storage, highlighting the importance of compressor efficiency

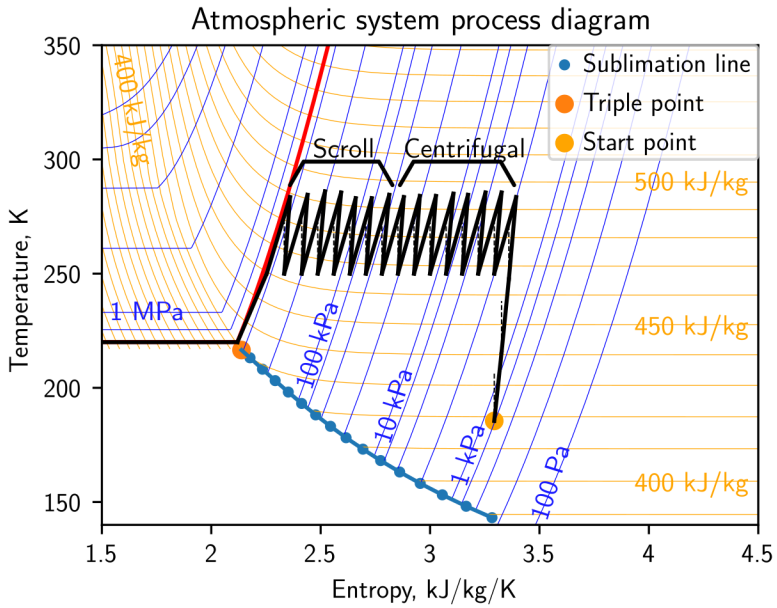

Figure 4.1: Temperature-entropy diagram of the optimum atmospheric resource acquisition process, with some salient features marked

improvements in reducing ESM and improving system performance. The compression work is split approximately evenly between centrifugal and scroll compressors (contributing 53% and 41% of total energy usage respectively). A similar split exists between heat rejection from intercooling and rejection from the condensing heat exchanger that liquefies the carbon dioxide before storage.

Subcomponent	Weight (kg)	Power (W_e)	Cooling Power (W_{th})
Axial weight	0.55		
Axial power		599.1	
Centrifugal weight	93.31		
Centrifugal power		6040.8	
Scroll weight	75.5		
Scroll power		4657.1	
HX weight	16.51		
HX pump power		52.46	
HX cooling			10650
Condenser weight	47.25		
Condenser power		7.88	
Condenser cooling			7875
Tank weight	34.25		
Total	**267.4**	**11357**	**18525**

Table 4.2: The properties of the optimal atmospheric system at design conditions

To explore the possible effect of the model errors identified in Section 3.2.4, a sensitivity analysis of the optimal atmospheric resource acquisition system was carried out. Each of 16 model parameters were individually increased by 10% and the effect on ESM was recorded with a new optimisation. These results are displayed in Figure 4.2. As is expected, varying the efficiency of centrifugal and scroll compressors has the largest effect on ESM, as these variables affect both the power and cooling of the system. Increasing mass flow by 10% increases ESM by less than

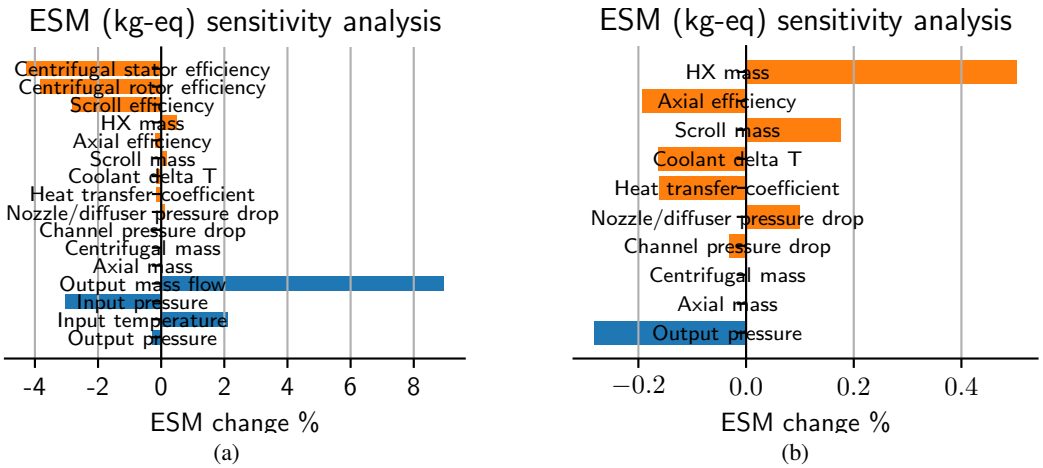

Figure 4.2: Sensitivity analysis for the Equivalent System Mass of a nominally optimal design. Each boundary condition or model variable is increased by 10% and the change in ESM is recorded

10%, demonstrating the overall favourable scaling of turbomachinery with mass flow.

When varying the ESM scaling factors to approximate the use of alternative auxiliary systems, the optimiser appropriately varied its internal prioritisation. With the baseline values of scaling factor from Table 2.2, very high importance is placed on reducing power and cooling as both are heavily penalised. Reducing these factors, as would be the case for a lightweight solar cell or radiator, causes the cost functions of each component to be less impacted by low efficiency and more by heavy components. This causes a slightly different machine to be optimal. Reducing the mass scaling of both power and cooling causes the optimal system mass to reduce by 12% while the power consumption increases by 7% and cooling by 5%. This shows how ESM scaling can be used as a simple lever to control the optimisation goals for an ISRU system.

With this complete description of the optimal system, a justification will now be made for it being the best possible. This includes the integration of this architecture versus alternatives into the rest of the ISRU stack, the choice of high-level architectural parameters and the choice of component designs.

4.2 Improvements of Integrated ISRU Plant

	Liquid feed		Gaseous feed	
	Atmospheric	Remainder	Atmospheric	Remainder
Mass (kg)	267.4	18144	116.8	18144
Power (kW_e)	9.99	1275	12.14	1497
Cooling (kW_{th})	18.26	351.5	6.2	462.4
Energy (kW h)	119.9	7650	68.9	8981
ESM total (kg)	293870		345070	

Table 4.3: The mass, power, cooling and energy storage demands of the water extraction, chemical processing and propellant liquefaction modules of a propellant production ISRU system. Values taken from scaling of [19] and [58].

As discussed in Section 3.1.3, it is possible to carry out an optimisation considering the integration of the atmospheric resource acquisition system with the rest of the ISRU plant. The

overall optimum design makes use of the atmospheric system to reduce some power and cooling demands from the ISRU stack's propellant liquefaction subsystem, reducing ESM substantially.

To determine the difference between optimising the atmospheric system with and without the rest of the ISRU stack, a comparative example is presented in Table 4.3. The 'liquid feed' system uses the optimum atmospheric system as described above, including a condensing heat exchanger and storage tank, while the 'gaseous feed' uses an atmospheric system that operates around the clock and does not liquify carbon dioxide. The former design uses the boiling and heating of carbon dioxide feed up to chemical reactor temperatures of around 600 K to chill the methane and oxygen products before they are fully liquefied by a cryocooler. This precooling substantially reduces the required cryocooler cooling power and thus energy input, mass and heat rejection, causing a large reduction in overall ISRU ESM. The impact of this liquid feed on ESM is actually four times larger than the impact of switching from a cryocooler to turbomachinery-based compression.

The 15% improvement in overall ISRU plant ESM clearly demonstrates the importance of optimisation with an appropriate system boundary. This relies on the use of a carbon dioxide condensing architecture - one which operates intermittently and stores carbon dioxide for use in the ISRU stack. Even with this restriction on architecture, there are many choices for mass flow and intercooler number. The next section discusses and justifies the particular architecture choice of the optimal design.

4.3 Architectural Design

Within the design space available, the design presented above has been selected as optimal. The choice of both intercooler number and mass flow is justified in this section by comparing the design to alternatives with different values for these parameters.

The architectural parameters of the optimised system are presented in Table 4.4. Using the design code written for this work, these variables are all that are needed to generate the full design. 15 intercoolers are used, which places the system at a high-efficiency low-mass point that minimises overall ESM. A mass flow of 22.5 g/s is used, the minimum allowed for a condensing system. The effect of varying the number of intercoolers on ESM will now be discussed, followed by the effect of varying mass flow.

Variable	Value	Requirement
Mass flow (g/s)	22.5	
Hours of daily operation	12	
Daily mass flow (kg/d)	1000	1000
Inlet pressure (Pa)	776	
Inlet temperature (K)	185	
Outlet pressure (kPa)	550	>500
Centrifugal/scroll compressor pressure ratio	1.502	
Number of intercoolers	15	
Intercooler outlet temperature (K)	250	
Intercooler log-mean temperature difference (K)	15	

Table 4.4: Architectural parameters for the optimised atmospheric resource acquisition system

The choice of number of intercoolers (and thus centrifugal/scroll compressor pressure ratio) balances the number and thus weight of components against the reduced specific work and (thus reduced power and cooling) from reduced average flow temperature. This trade-off is shown in

Figure 4.3, particularly 4.3a where the balance of mass and Equivalent System Mass of power and cooling are compared. An intercooler number of 15 is at an optimum for both mass but also power - at higher intercooler numbers, the pressure drop of the intercooling heat exchangers raises the required compression work. The irregular variation of system mass is due to variation in the discrete numbers of centrifugal and scroll compressors, shown in Figure 4.3b.

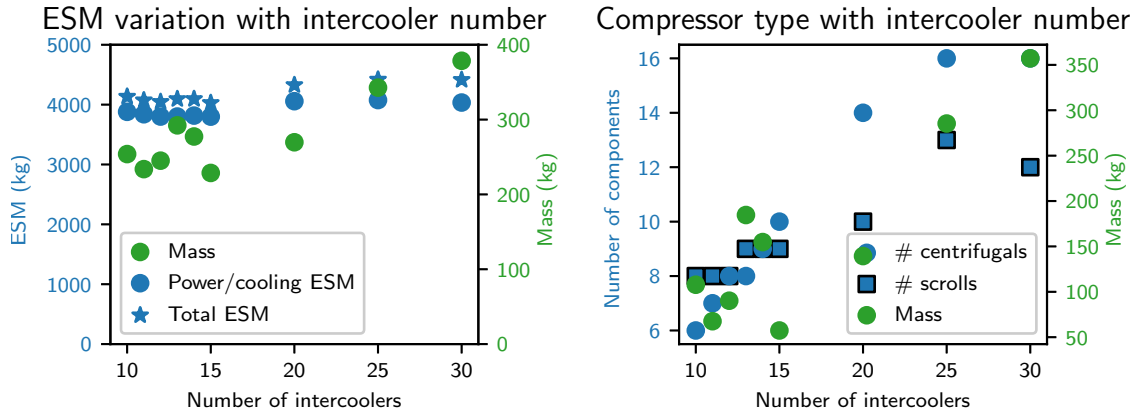

(a) Variation in the mass, equivalent system mass of power and cooling, and total ESM of the atmospheric system with number of intercoolers

(b) Variation in the number of centrifugal and scroll compressors, and total system mass, with number of intercoolers

Figure 4.3: Variation in system performance with a variation in the number of intercoolers. Mass flow is held constant at 22.5 g/s, and all other architectural parameters are held at the same values as the optimum system.

A similar analysis can be carried out with changes to mass flow through the system. The variation of ESM with mass flow shows less complex behaviour - mass, power and cooling all increase approximately linearly as mass flow increases. However, all of these performance characteristics have slopes of less than one. This is a strong indication of the favourable scaling laws associated with the system architecture chosen. The gradient of the ESM-mass flow line is around 0.5, such that doubling mass flow causes a roughly 50% increase in ESM. Thus, if the chosen optimisation metric was ESM per unit mass flow (some sources use kg/(kg/h) for this value), the correct approach would be to maximise mass flow.

A number of variables contribute to this scaling law. Firstly, larger mass flows require larger turbomachinery with larger blade spans, less passage blockage from boundary layers and less tip clearance. This means that the lighter, more efficient centrifugal compressors can be used to a higher pressure and fewer heavy, inefficient scroll compressors are needed. As mass flow increases from the optimal 22.5 g/s to the maximum considered 90 g/s, the number of centrifugal compressors in an optimum design increases from eight to ten and the number of scroll compressors falls from seven to five. This increases overall efficiency and reduces specific compression energy, as seen in Figure 4.4b.

4.4 Component Design

The effectiveness of the component optimiser at producing suitable designs will now be discussed briefly. The optimiser performed well, with efficient components produced using a minimal number of function calls and thus a quick optimisation time.

The component optimisation system, as implemented with the method discussed above, worked very effectively to produce suitable components throughout the optimised system. The optimiser reliably produced systems with an average compressor efficiency above 60% and a pressure

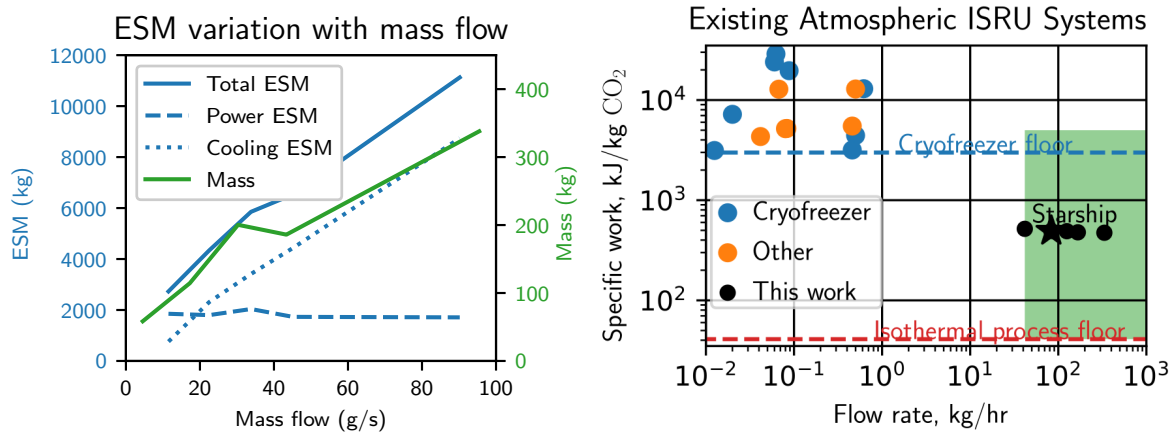

(a) Variation in the mass, equivalent system mass of power and cooling, and total ESM of the atmospheric system with mass flow through the system.

(b) Variation in specific compression work with mass flow, comparing this work to existing literature. Data from literature from Figure 1.3

Figure 4.4: Variation in system performance with a variation in the mass flow. The number of intercoolers is held at 15, and all other architectural parameters are held at the same values as the optimum system.

drop in each heat exchanger of 5% of dynamic head or less. A typical optimisation run with fifteen intercoolers and thus 36 components took around ten seconds to execute, with around 100 variables optimised over. With 2-3 optimisations needed per system designed (to adjust the output pressure of the system towards a target value), 25 systems designed and 4 combinations of ESM scaling factor assessed, the entire design evaluation process of 250 optimisation runs took around 40 minutes to complete.

To determine the effectiveness with varying optimisation speed, the tolerance of the Nelder-Mead algorithm (the difference between each function evaluation before convergence was declared) was varied across seven orders of magnitude and compared. The ESM of the designed component was compared with the minimum from a brute-force search of 250,000 evaluated designs in the relevant operating regime. An intermediate tolerance value achieved an ESM within 0.2% of the best value found in the exhaustive search, with a 60-fold improvement in execution time compared to the search. This is shown in Figure 4.5.

4.4.1 CFD Validation

To explore the accuracy of the efficiency prediction of the nominally system, CFD was carried out on select centrifugal compressors. The TBLOCK code, with appropriate meshing codes for centrifugal impellers and diffusers was used as described above. The first and last centrifugal compressor in the optimal design were modelled and simulated with a coarse design mesh. Some select images of this analysis, created using Paraview, are shown in Figure 4.7. Unwrapped views through the impeller of each, plotted in Python, are in Figures 4.8 and 4.9.

To determine if the optimiser was indeed selecting a point near the optimum, some geometric parameters (diffuser angles and radius, inlet and outlet blade span, inlet hub radius) were varied. The change in efficiency from varying each of these parameters by ±5% is shown in Figure 4.6. This shows that the impeller optimisation is performing well, with the variations in geometry causing a drop in efficiency. However the optimisation of the diffuser angle is particularly poor. The likely cause of this is a poor matching of length to throat width ratio in the CFD, which did not account for this with the choice of diffuser blade number. As can be seen in Figure 3.4a, varying angle at constant area ratio can cause considerable changes in efficiency and length to throat width ratio.

The efficiencies of both compressors in CFD was at least 10 percentage points lower than predicted by the model. The most plausible causes of this are the arbitrary choice of blade number in both the impeller and diffuser, which were not output by the component model. A bad choice of blade number in either the impeller or diffuser would cause separation and secondary flows, some of which were observed near impeller outlet.

The CFD validation shows that the model is fairly accurate in predicting the location of the maxima and thus the final design is likely to be close to the true optimum, even if the merit is different. It again highlights that the diffuser model is somewhat problematic and could be leading to an underestimation of the achievable efficiency of the centrifugal compressors uses in the atmospheric resource acquisition system. Addressing the issues with this model would be a priority for future work.

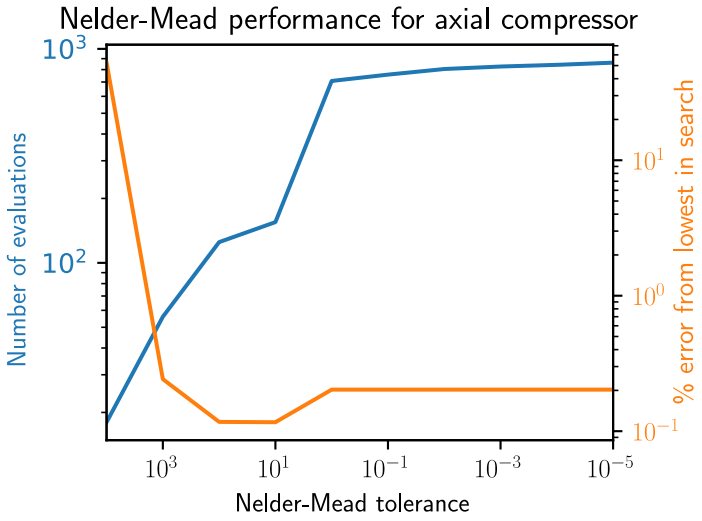

Figure 4.5: Error between brute-force search, and number of function evaluations, for a Nelder-Mead component optimisation with varying tolerance

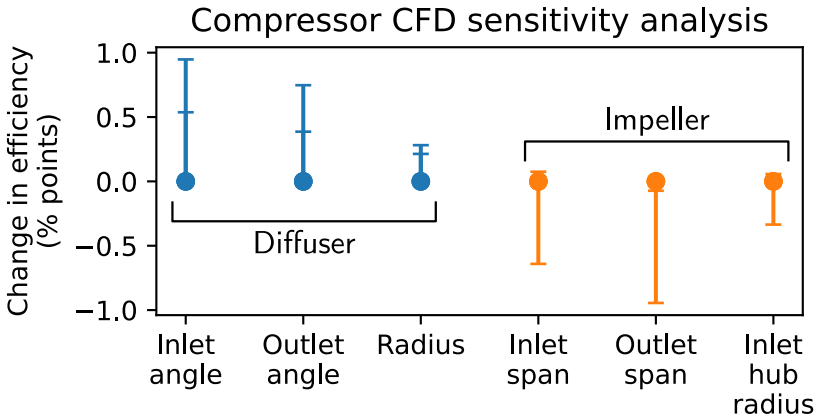

Figure 4.6: CFD calculations of the change in efficiency (percentage points) from varying the value of select geometric parameters by plus or minus 5%

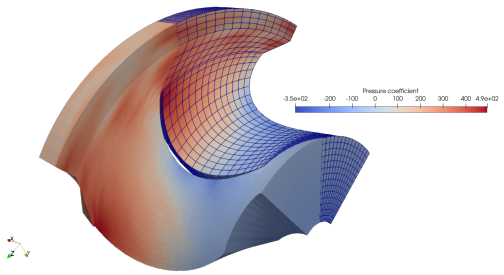

(a) First centrifugal compressor, impeller view

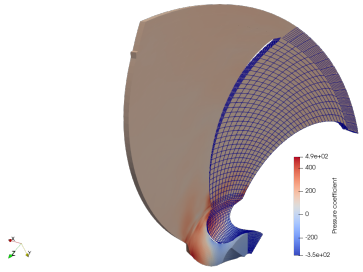

(b) First centrifugal compressor, whole view

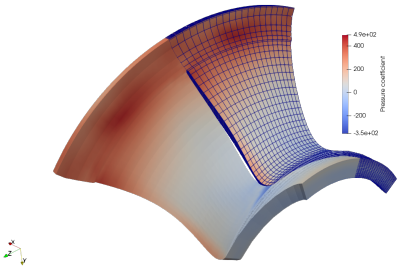

(c) Last centrifugal compressor, impeller view

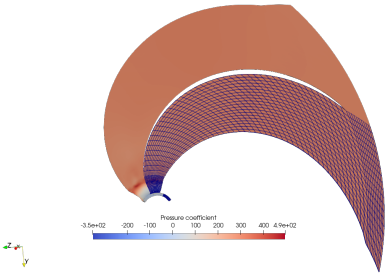

(d) Last centrifugal compressor, whole view

Figure 4.7: Select images of the CFD analysis. All plotted with pressure rise coefficient, the difference between static pressure and inlet total pressure over diffuser exit dynamic pressure. Pressure rise coefficient in the impeller of both compressors varies from -350 to 500. Pressure rise coefficient in the diffuser of both is roughly constant at 250-300

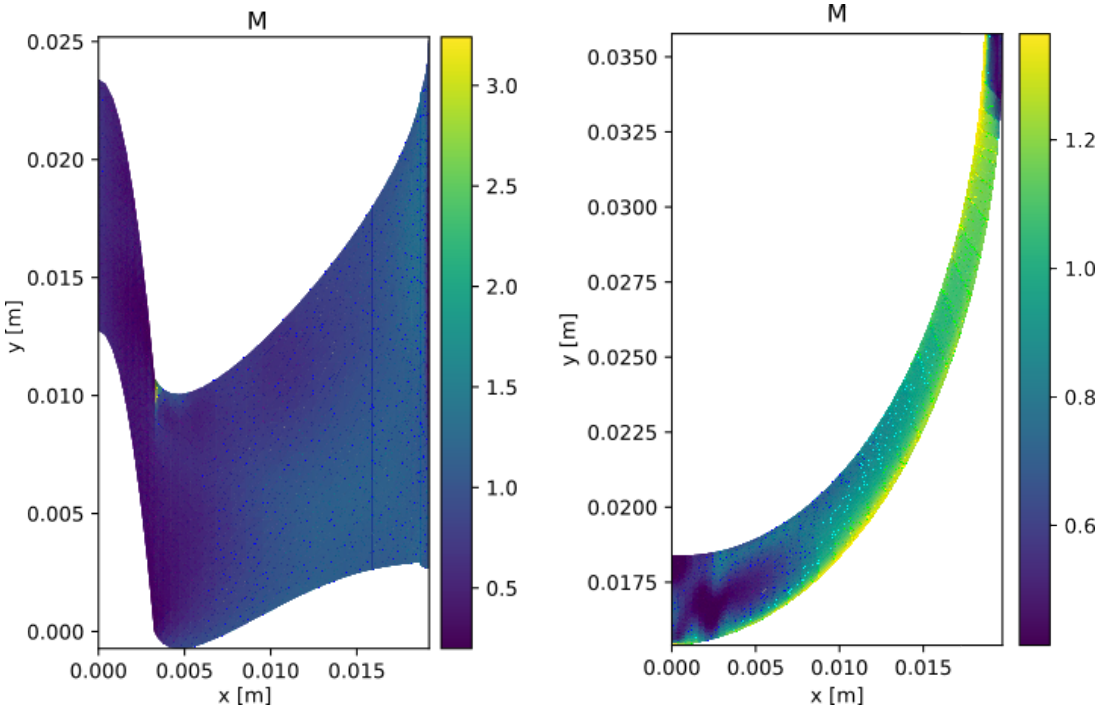

Figure 4.8: Low-pressure impeller cross-section, unwrapped around the $r\theta$ axis, and through the centre of the passage. Both plots coloured by Mach number

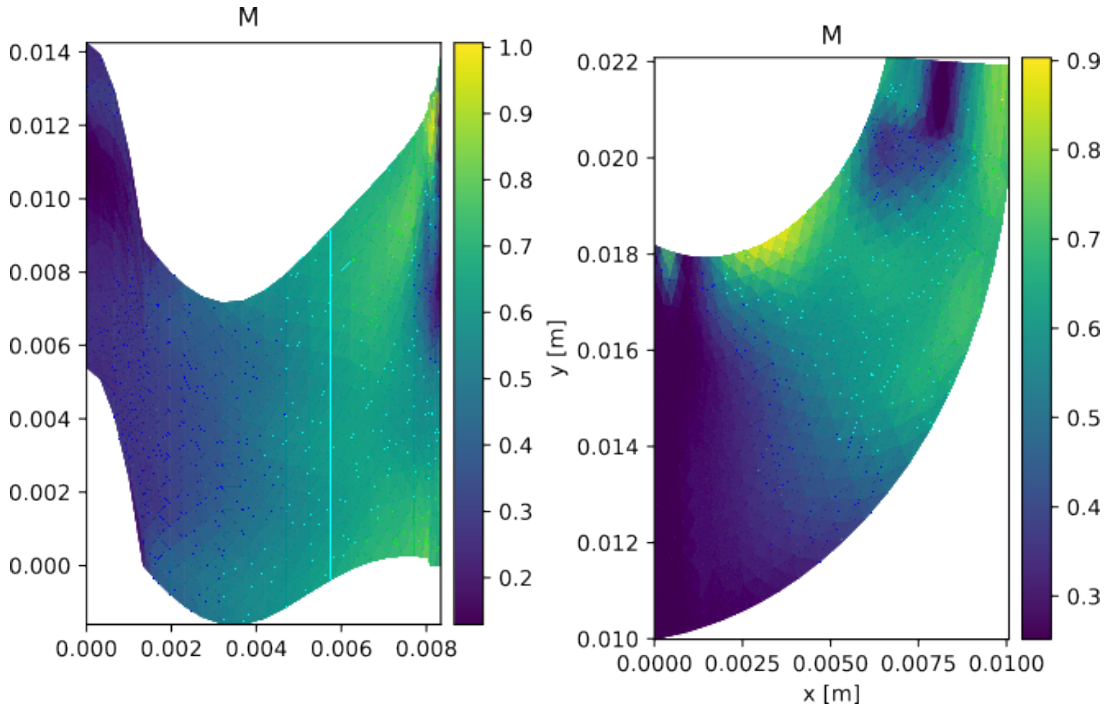

Figure 4.9: High-pressure impeller cross-section, unwrapped around the $r\theta$ axis, and through the centre of the passage. Both plots coloured by Mach number

5 Implications and Future Work

The successful preliminary design of an atmospheric resource acquisition system has several implications for the design of other Martian systems in the near future, beyond the immediate propellant ISRU application. However, there are also many avenues of future work that would improve and build upin these results.

5.1 Cost of Carbon Dioxide

The most significant impact of this work is a four-fold reduction of the 'cost' of carbon dioxide in Martian ISRU at Starship scale. This has a direct impact on the design of next-generation ISRU plants, as less power and mass needs to be allocated to atmospheric resource extraction. This could allow for increased system reliability through hardware redundancy of components or increased mass and power budgets for other payloads.

This benefit is increased further for carbon dioxide-rich ISRU processes, such as solid oxide electrolysis. The atmospheric resource acquisition subsystem comprises a larger fraction of ESM for these processes, so a reduction in carbon dioxide cost is more impactful.

Encouragingly for future human Mars programs, this work suggests that the cost of carbon dioxide decreases as mass flows increase, thanks to the favourable scaling laws for compressor mass and efficiency. This implies that the larger mass flows required for permanent Mars settlement and 'colonisation' would be delivered both at lower mass and power costs than previously assumed, and at increasingly low costs as the scale of operations on the red planet grows.

5.2 Wider Applications

This work provides some credibility to the concept of turbomachinery as a viable technology for Martian atmospheric resource acquisition, and suggests that high-pressure carbon dioxide could be a low-cost resource in a future Martian industrial system. Beyond the application of ISRU for propellant production, low-cost carbon dioxide has a number of other proposed uses on Mars.

England and Hrubes [59] have proposed the use of a large turbomachinery-based system for simultaneous power generation and atmospheric ISRU. Their MARRS proposal uses compression of the Martian atmosphere to liquefaction pressure and fractional distillation of the permanent gases to produce a supply of oxygen, nitrogen and argon. The remaining liquid carbon dioxide is heated by a nuclear reactor and expanded through turbines to both drive the compressors and provide electrical power to a habitat. This work's model for turbomachinery compressors could be used to support such an open-cycle power generation concept.

Another possibility that utilises low-cost liquid carbon dioxide is providing effective cooling throughout an industrial system. Carbon dioxide can be liquefied at a central atmospheric processing plant and transported easily. This liquid could then be boiled, to provide cooling to low temperatures (down to 210 K) and high heat transfer rates.

Finally, low-cost carbon dioxide is a valuable feedstock for other ISRU processes. These range from plastic production to agriculture, and collectively form the backbone of a future Martian industrial stack. Atmospheric resources ultimately provide all of the carbon and nitrogen, and much of the oxygen, for this stack, and so reducing the cost of carbon dioxide represents a very significant step in reducing the energy and mass costs of Martian industry in general.

5.3 Future Work - Advanced Optimisation

The optimisation of the turbomachinery and intercooling heat exchangers in this thesis is relatively simple, enabling rapid evaluation of many architectures. A significant route for future work would be to improve the accuracy and fidelity of this optimisation by refining the models.

The most obvious avenue for improving the optimisation of the overall system is modifying the calculation of efficiency of axial and centrifugal compressors. The use of the Smyth and Miller model makes a number of simplifying assumptions about the geometry, Mach number, tip gap, working fluid and blade number. An improved calculation might improve the calculation with more granular correlations accounting for different loss mechanisms, or better yet introduce appropriate CFD into the process. This could take the form of using CFD to produce Smyth and Miller plots for the relevant regimes of each compressor, or using a more advanced optimiser than Nelder-Mead to allow for fewer function iterations and thus enable CFD to be used directly in the optimisation of each component. Currently a flat 15% efficiency decrement is applied to all centrifugal compressors to roughly match computational results - if this decrement could be reduced through appropriate optimisation, a considerable reduction in the energy cost of carbon dioxide could be achieved.

Additionally, no specific optimisation of blade geometry or number was carried out as part of this work, and could provide ample routes for further improvements of both compressor efficiency and weight. Particularly in the case of centrifugal compressors, very generic models were used for geometry in the impeller and diffuser, and it would almost certainly be possible to improve on overall performance with appropriate variation of flow turning and exit manifolds/volutes. The particular coupling of centrifugal compressors to intercooling heat exchangers could also be explored, potentially including cooling within the diffuser to partially combine the heat exchanger and compressor components.

Also, no consideration has been given in this analysis to the startup process or general off-design behaviour of the multistage compressor. This may be substantially easier than for traditional compressor-driven systems in terrestrial applications because of the likely application of direct electric drive, thus allowing for variable speed on each compressor during the startup process. Similarly, the off-design performance of each compressor could be analysed to help determine the off-design performance of the whole machine. The variable-speed per-stage electric drive would simplify the part-speed matching problem in multistage axial compressors but the extremely high overall pressure ratio may still cause complexities with surge during startup or flow perturbations. Relatedly , a general design or optimisation of the electric drive for the entire compressor system could be carried out. This was considered beyond the scope of this work due to a lack of available literature on the possible performance envelope of high-speed low-weight electric motors.

5.4 Future Work - Design Integration

In order to drive improvements in the ISRU system as a whole, the design optimisation of the atmospheric resource acquisition system can be further coupled to the downstream electrochemical processing and other auxiliary subsystems.

Some aspects of the atmospheric resource acquisition system not directly necessary to the core compression have been modelled simply, including the dust handling equipment and final condensing heat exchanger. Since the design of each of these subsystems is largely invariant as the compressor stack is optimised, this simple model likely does not affect the optimal design point but does affect the final merit of the optimised system. The optimisation of both of these

sybsystems would likely require more advanced correlation-based design or CFD.

In addition to this, the optimisation of the atmospheric acquisition system could be coupled to a model of the electrochemical processing systems. In particular, the effectiveness and yield of the chemical process is likely closely coupled to the pressure and temperature of the inlet gases. If the pressure of the chemical reactor can be reduced, the pressure ratio of the compressor and thus energy requirements could be substantially reduced - although this may preclude the use of liquid carbon dioxide if the reactor pressure is substantially below the triple point of carbon dioxide.

Similarly, one avenue for potential system-level optimisation involves the coupling of the atmospheric system's heat rejection to low-temperature endothermic processes. The most obvious of these is the melting of ice, which provides a heat sink at temperatures around 200 K that may be very well-utilised for cooling the intercooling heat exchangers. This requires a much broader scope of optimisation with considerations for the operations, practicality and cost of an ISRU operation.

It may well be the case that any more advanced optimisation of the ISRU process to operate on Starship would require such a scope for optimisation that it may not be possible to carry out without a more complete understanding of the Starship Mars mission concept of operations. This may require the usage of a Design Reference Architecture-type document for Starship, which does not currently exist in the public domain and would require a great deal of propietary information from SpaceX.

5.5 At-Scale vs Scalable Designs

Aside from the specific outcomes of this work in improving the effectiveness of Martian atmospheric resource acquisition systems, it stands as an example of the paradigm of thinking that may be required for large-scale Martian and space settlement. Unlike traditional designs for ISRU process engineering, which focus on demonstrating a systems architecture at small scale before scaling up, the atmospheric system described here is fundamentally nonviable at small scales. Axial and centrifugal compressors cannot be made arbitrarily small due to limits of tolerance and tip clearances, and the architecture of intercooling heat exchanger described similarly become unfeasible to manufacture when made extremely small. The only component that could be effectively used for a subscale demonstrator is the scroll compressor - hence the application in small experiments like MOXIE.

This illustrates the difference between designing a scalable and at-scale system. A scalable architecture (for instance, one reliant on scroll compressors) could be tested at small scales in a lab or on demonstrator missions, but cannot achieve the same efficiencies as turbomachinery. In choosing an architecture than can be scaled and tested in this way, the designers of ISRU systems are implicitly blocking themselves from areas of the design space that would otherwise be advantageous. Designing instead at full scale carries greater design risk and cost, as no subscale tests can be carried out, but allows much more effective architectures to be used.

This difference between designing systems that are scalable, versus designing systems to work at-scale, extends across domains of space engineering from habitat design to transport systems to ISRU process engineering. It is hoped that this thesis will serve as an example of the improvements in efficiency, cost and effectiveness that can be achieved by first considering the at-scale system when designing a system to serve humanity over the next decades of space exploration and settlement.

6 Conclusion

To carry out a successful Mars mission with reasonable cost and complexity, in-situ resource utilisation to produce propellant is required. The operation of ISRU at large scales requires the design and use of large-scale resource acquisition and processing systems, far beyond the scale of current technologies. This work carries out the preliminary design of one subsystem for the ISRU plant, the atmospheric resource acquisition system. Through the use of turbomachinery, lightweight intercoolers and careful optimisation a four-fold improvement over the current-state-of-the-art has been achieved. This demonstrates the effectiveness of the two-level design process used, and of the gain in performance possible with large-scale thinking in ISRU engineering.

A Risk Assessment Retrospective

As this was an entirely computational project, the only risks originally identified were those associated with prolonged computer use (injury due to poor posture, etc). Through appropriate controls, no injuries of this type occured, and no other hazards were present.

B Nomenclature

Abbreviations

ESM	Equivalent System Mass
ISRU	In-Situ Resource Utilisation

Subscripts

0	Stagnation properties
1	Inlet of component
2	Outlet of compressor impeller
3	Inlet of compressor diffuser
4	Outlet of compressor diffuser
d	Heat exchanger diffuser
h	Hub
m	Mean line
n	Heat exchanger nozzle
q	Heat exchanger main section
t	Tip
w	Wall
x	Axial direction

Symbols

Δh	Specific enthalpy change [J/kg]
$\dot{m}$	Mass flow [kg/s]
η	Efficiency
Ω	Rotational speed [rad/s]
ρ	Density [kg/m^3]
A	Area [m^2]
b	Blade span [m]
d	Diameter [m]
f	Friction factor
L	Length [m]
P	Electrical power [W$_e$]
p	Pressure [Pa]
Q	Heat flux [W$_{th}$]
R	Radius [m]
s	Pitch [m]
T	Temperature [K]
t	Thickness [m]
U	Blade speed [m/s]
V	Flow velocity [m/s]
W	Weight [kg], Relative velocity [m/s]
M	Mach number
Pr	Prandtl number
Re	Reynolds number

C Acknowledgements

I want to thank everyone who's supported me throughout the writing of my Master's thesis. This must include Professor Nick Atkins, who's been an immense help with all matters turbomachinery, and in guiding my research process to produce this work. Many others in the Whittle Laboratory at Cambridge have provided useful input and discussion over the year. Thanks also go to Paul Wooster of SpaceX for suggesting atmospheric ISRU as a topic, and to Eric Hinterman of MIT/SpaceX and Michael Hecht of MIT for enlightening conversations on broader ISRU topics. I am grateful to all my friends at Cambridge and my parents for enduring endless discussion of Mars. And finally, thanks to Lucy, who's been at my side every step of the way.

References

[1] W. von Braun. *Manned Mars Landing: Presentation to the Space Task Group*. Presentation. National Aeronautics and Space Administration, 1969.

[2] S. J. Hoffman and D. I. Kaplan. *Human Exploration of Mars: The Reference Mission of the NASA Mars Exploration Study Team*. Special Publication NASA-SP-6107. Lyndon B. Johnson Space Center, Houston, TX, USA: National Aeronautics and Space Administration, 1993.

[3] B. G. Drake et al. *Human Exploration of Mars Design Reference Architecture 5.0*. Special Publication NASA-SP–2009–566. National Aeronautics and Space Administration, 2009.

[4] Accessed: 2023-05-27. URL: https://www.spacex.com/vehicles/starship/.

[5] M. Anderson et al. *Life Support Baseline Values and Assumptions Document*. 2015.

[6] Julie E. Kleinhenz and Aaron Paz. "An ISRU propellant production system for a fully fueled Mars Ascent Vehicle". In: *10th Symposium on Space Resource Utilization* (2017). DOI: 10.2514/6.2017-0423.

[7] R.L Ash, W.L Dowler, and G Varsi. "Feasibility of rocket propellant production on Mars". In: (1978). DOI: 10.1016/0094-5765(78)90049-8.

[8] R. Zubrin and R. Wagner. *The case for Mars: The plan to settle the Red Planet and why we must*. 2021.

[9] M Golombek et al. "SpaceX Starship Landing Sites on Mars". In: *52nd Lunar and Planetary Science Conference*. 2021.

[10] Anthony Muscatello and Edgardo Santiago-Maldonado. "Mars in situ Resource Utilization Technology Evaluation". In: *50th AIAA Aerospace Sciences Meeting including the New Horizons Forum and Aerospace Exposition* (Jan. 2012). DOI: 10.2514/6.2012-360.

[11] E. F. Meyen. "System Modeling, Design, and Control of the Mars Oxygen In-Situ Resource Utilization Experiment (MOXIE) and Implications for Atmospheric ISRU Processing Plants". PhD thesis. May 2017.

[12] Jeffrey A. Hoffman et al. "Mars Oxygen ISRU experiment (moxie)—preparing for human mars exploration". In: *Science Advances* (Sept. 2022). DOI: 10.1126/sciadv.abp8636.

[13] Abdul M. Ismail. "Technology requirements for Mars sample return using CO2/Metal Powder Propellants". In: *54th International Astronautical Congress of the International Astronautical Federation* (Sept. 2003). DOI: 10.2514/6.iac-03-q.3.b.06.

[14] Joseph Trevathan, Kevin Payne, and David Clark. "Carbon dioxide collection and purification system for Mars". In: *AIAA Space 2001 Conference and Exposition* (Aug. 2001). DOI: 10.2514/6.2001-4660.

[15] D. Rapp et al. "Preliminary system analysis of in situ resource utilization for mars human exploration". In: *2005 IEEE Aerospace Conference* (2005). DOI: 10.1109/aero.2005.1559325.

[16] A. Muscatello, R. Devor, and J. Captain. "Atmospheric Processing Module for mars propellant production". In: *Earth and Space 2014* (June 2015). DOI: 10.1061/9780784479179.047.

[17] Shah Saud Alam et al. "Thermodynamic modeling of in-situ rocket propellant fabrication on Mars". In: *iScience* (May 2022). DOI: 10.1016/j.isci.2022.104323.

[18] Hao Chen et al. "Integrated in-situ resource utilization system design and logistics for Mars Exploration". In: *Acta Astronautica* (May 2020). DOI: 10.1016/j.actaastro.2020.01.031.

[19] Robert M. Zubrin, Anthony C. Muscatello, and Mark Berggren. "Integrated Mars in situ Propellant Production System". In: *Journal of Aerospace Engineering* (2013). DOI: 10.1061/(asce)as.1943-5525.0000201.

[20] Donald Rapp. *Use of extraterrestrial resources for human space missions to Moon or Mars*. Springer International, 2019.

[21] Eric Hinterman. "Multi-Objective System Optimization of a Mars Atmospheric ISRU Plant". PhD thesis. May 2022.

[22] Paul Wooster. Personal communication. SpaceX. Dec. 2021.

[23] François Forget et al. "Improved general circulation models of the Martian atmosphere from the surface to above 80 km". In: (1999). DOI: 10.1029/1999JE001025.

[24] J. Levri et al. *Advanced Life Support Equivalent System Mass Guidelines Document*. Technical Memorandum NASA-TM–2003–212278. National Aeronautics and Space Administration, 2003.

[25] A. J. Hanford and M. K. Ewert. *Advanced Active Thermal Control Systems Architecture Study*. Technical Memorandum NASA-TM-104822. Johnson Space Center, Houston, TX, USA: National Aeronautics and Space Administration, 1996.

[26] I. H. Bell et al. "Pure and Pseudo-pure Fluid Thermophysical Property Evaluation and the Open-Source Thermophysical Property Library CoolProp". In: (2014). DOI: 10.1021/ie4033999.

[27] M. P. Vukalovich. *Thermophysical properties of carbon dioxide*. 1968.

[28] M. G. Tomasko et al. "Properties of dust in the martian atmosphere from the imager on Mars pathfinder". In: *Journal of Geophysical Research: Planets* (1999). DOI: 10.1029/1998je900016.

[29] F. Forget and L Montabone. "Atmospheric Dust on Mars: A Review". In: *47th International Conference on Environmental Systems* (2017).

[30] Ruth F. Weiner, Robin A. Matthews, and P. Aarne Vesilind. "Air Pollution Control". In: *Environmental engineering*. Butterworth-Heinemann, 2003, pp. 385–408.

[31] C. B. Shephered and C. E. Lapple. "Flow pattern and pressure drop in Cyclone dust collectors". In: *Industrial and Engineering Chemistry* (Aug. 1939). DOI: 10.1021/ie50356a012.

[32] C I Calle et al. "Electrostatic precipitation of dust in the martian atmosphere: Implications for the utilization of resources during future manned exploration missions". In: *Journal of Physics: Conference Series* (Dec. 2011). DOI: 10.1088/1742-6596/327/1/012048.

[33] Juan Antonio Bravo-Aranda et al. "Study of mineral dust entrainment in the planetary boundary layer by lidar depolarisation technique". In: *Tellus B: Chemical and Physical Meteorology* (2015). DOI: 10.3402/tellusb.v67.26180.

[34] Royce N. Brown. In: *Compressors: Selection and sizing*. Gulf, 1997, pp. 3–4.

[35] Jonathan M. Smyth and Robert J. Miller. "Selecting a compressor meridional topology: Axial, Mixed, radial". In: *Volume 2C: Turbomachinery — Design Methods and CFD Modeling for Turbomachinery; Ducts, Noise, and Component Interactions* (2021). DOI: 10.1115/gt2021-59121.

[36] Joe Hartsvigen. Personal communication. OxEon Energy. Feb. 2023.

[37] R Miller and J Taylor. *Lecture notes in Turbomachinery*. Oct. 2023.

[38] D. A. Sagerser, S. Lieblein, and R. P. Krebs. *Empirical expressions for estimating length and weight of axial-flow components of VTOL powerplants*. Technical Memorandum NASA-TM-X-2406. Lewis Research Center, Cleveland, OH, USA: National Aeronautics and Space Administration, 1971.

[39] L. R. Reneau, J. P. Johnston, and S. J. Kline. "Performance and design of straight, two-dimensional diffusers". In: *Journal of Basic Engineering* (Mar. 1967). DOI: 10.1115/1.3609544.

[40] Michael Casey and Chris Robinson. "Radial flow Turbocompressors". In: (2021). DOI: 10.1017/9781108241663.

[41] Accessed: 2023-05-28. URL: https://airsquared.com/products/scroll-compressors/.

[42] Yangguang Liu, Chinghua Hung, and Yuchoung Chang. "Design optimization of scroll compressor applied for frictional losses evaluation". In: *International Journal of Refrigeration* (May 2010). DOI: 10.1016/j.ijrefrig.2009.12.015.

[43] Y-H Cho, B-C Lee, and J-K Lee. "Development of High Efficiency Scroll Compressor for Package Air Conditioners". In: *International Journal of Refrigeration* (1996).

[44] Richard Varvill. "Heat exchanger development at Reaction Engines Ltd.." In: *Acta Astronautica* (2010). DOI: 10.1016/j.actaastro.2009.11.010.

[45] Yunus A. Cengel. *Heat transfer: A Practical approach*. McGraw-Hill, 2007.

[46] Accessed: 2023-05-29. URL: https://www.engineeringtoolbox.com/minor-loss-air-ducts-fittings-d_208.html.

[47] Fuchang Gao and Lixing Han. "Implementing the Nelder-Mead simplex algorithm with adaptive parameters". In: *Computational Optimization and Applications* (May 2010), pp. 259–277. DOI: 10.1007/s10589-010-9329-3.

[48] Sam Ross. *TurboMars: Martian Turbomachinery Analysis Code*. Version 0.1.0. May 2023. URL: https://github.com/smross106/TurboMars.

[49] R. D. Moore and L. Reid. *Design and overall performance of four highly loaded, high speed inlet stages for an advanced high-pressure-ratio core compressor*. Technical Paper NASA-TP-1337. Lewis Research Center, Cleveland, OH, USA: National Aeronautics and Space Administration, 1978.

[50] R. J. Steinke. *Design of 9.271-pressure-ratio 5-stage core compressor and overall performance for first 3 stages*. Technical Paper NASA-TP-2597. Lewis Research Center, Cleveland, OH, USA: National Aeronautics and Space Administration, 1986.

[51] J. P. Veres and D. R. Thurman. *Conceptual Design of a Two Spool Compressor for the NASA Large Civil Tilt Rotor Engine*. Conference Paper NASA-E-17251. Glenn Research Center, Cleveland, OH, USA: National Aeronautics and Space Administration, 2010.

[52] Fangyuan Lou, John C. Fabian, and Nicole L. Key. "A new approach for centrifugal impeller preliminary design and aerothermal analysis". In: *Journal of Turbomachinery* (Feb. 2018). DOI: 10.1115/1.4038876.

[53] J. Wood, P. Adam, and A. Buggele. "NASA low-speed centrifugal compressor for fundamental research". In: *19th Joint Propulsion Conference* (June 1983). DOI: 10.2514/6.1983-1351.

[54] Lixin Cheng and Cees W. Geld. "Experimental study of heat transfer and pressure drop characteristics of air/water and air-steam/water heat exchange in a polymer compact heat exchanger". In: *Heat Transfer Engineering* (Feb. 2005). DOI: 10.1080/01457630590897033.

[55] Minsung Kim et al. "Experimental study on corrugated cross-flow air-cooled plate heat exchangers". In: *Experimental Thermal and Fluid Science* (June 2010). DOI: 10.1016/j.expthermflusci.2010.05.007.

[56] John Denton and Graham Pullan. *TBLOCK 7.5 Parallel2.0*. Aug. 2009.

[57] Developed by Dr Nick Atkins at the Whittle Laboratory.

[58] Stephen J. Hoffman, Alida D. Andrews, and Kevin D. Watts. "Simulated water well performance on Mars". In: *2018 AIAA SPACE and Astronautics Forum and Exposition* (2018). DOI: 10.2514/6.2018-5293.

[59] J. D. Hrubes and C. England. *Mars Atmosphere Resource Recovery System (MARRS)*. http://web.archive.org/web/20201111212251/https://www.niac.usra.edu/files/studies/final_report/483England.pdf. 2001.